Development of Cell-Permeable, Water-Soluble, Peptide-Based Fluorescent Sensors for Detection of Analytes in a Biological System

A Thesis

Submitted to

Indian Institute of Science Education and Research Pune in partial fulfilment of the requirements for the BS-MS Dual Degree Programme

by

Ranojoy Baisya
20191008

Indian Institute of Science Education and Research Pune

Dr. Homi Bhabha Road,

Pashan, Pune 411008, India

March, 2024

Supervisor: Prof Ankona Datta

Department of Chemical Sciences, Tata Institute of Fundamental Research, Mumbai

Certificate

This is to certify that this dissertation entitled “Development of Cell-Permeable, Water-Soluble, Peptide-Based Fluorescent Sensors for Detection of Analytes in a Biological System” towards the partial fulfilment of the BS-MS dual degree programme at the Indian Institute of Science Education and Research, Pune represents study/work carried out by Ranojoy Baisya at Tata Institute of Fundamental Research, Mumbai under the supervision of Prof Ankona Datta, Department of Chemical Sciences, during the academic year 2023-2024.

Ankona Datta

Prof Ankona Datta

Committee:

Prof Ankona Datta

Prof S. G. Srivatsan

This Thesis is Dedicated to My Parents and Brother

Declaration

I hereby declare that the matter embodied in the report entitled “Development of Cell-Permeable, Water-Soluble, Peptide-Based Fluorescent Sensors for Detection of Analytes in a Biological System” are the results of the work carried out by me at the Department of Chemical Sciences, Tata Institute of Fundamental Research, Mumbai, under the supervision of Prof Ankona Datta and the same has not been submitted elsewhere for any other degree. Wherever others contribute, every effort is made to indicate this clearly, with due reference to the literature and acknowledgement of collaborative research and discussions.

Ranojoy Baisya

Ranojoy Baisya
Roll: 20191008
Date: 14.04.2024

Acknowledgement

I am delighted to offer my heartfelt gratitude to Prof Ankona Datta, my project supervisor, for providing me with the chance to work and use the cutting-edge fundamental research resources at TIFR. Prof Datta provided an environment in which I could make mistakes, learn from them, and develop as a researcher, so improving my ability to think independently. This diverse experience was really beneficial to my learning and development as a researcher. Prof Ankona Datta also taught me that failure is typical in research and that it is permissible to repeat experiments several times. She also taught me essential skills, such as how to improve my writing and presentation skills and how to build a solid profile for graduate opportunities outside of India.

I am grateful to Prof. S.G. Srivatsan, a member of my TAC, for his steadfast support throughout difficult times. Despite his busy schedule, he patiently listened and pushed me to think about the project's future prospects. I also appreciate the aid of my current lab colleagues, who have always been available to help me manage the challenges of the new lab setting. Their efforts have helped to preserve a stress-free and happy working environment. Furthermore, I appreciate the assistance and stress-free chats with our lab's technical officer, Deepika Rao, who has been helpful in diagnosing issues.

I'd also want to thank my counselor, Vrinda, for listening to me at difficult moments and assisting me in finding solutions on my own. I'd also like to thank Anvi for providing me with invaluable insights into the realities of Indian academia and assisting me in navigating and solving challenges. I will be eternally grateful to my parents and brother for being my rock, offering consistent love, care, and nurturing. Finally, a special thank you to my pals Hritwik, Pritam, Shayandeep, Ankan, Souvik, and Rahul for being stress relievers and persistent supporters throughout my time at IISER.

Ranojoy Baisya

Table of Contents

Abstract

Non-genetically encoded analytes like metal ions, anions, reactive oxidative species, protons, sugar, lipids, and others are extremely crucial for proper functioning of the biological system. However, the distribution and localization of these analytes change both spatially and temporally and these spatio-temporal dynamics are important for key life-processes. Disruptions in the same can lead to severe pathophysiological conditions. Moreover, the distribution and localizations of one analyte is often functionally or structurally related to the dynamics of other analytes present in the biological milieu. In order to understand the inter-relationships between various analytes, we need to visualize these analytes simultaneously within different intracellular compartments. The primary objective of this thesis was to design and develop peptide-derived fluorescent tools. These tools were intended to enable the simultaneous tracking of proton concentration and hydrogen peroxide levels, both of which are critical analytes within biological systems, specifically within autophagic vesicles and mitochondria.

List of Figures

ABBREVIATIONS

1. AIM: Atg8- interacting motif
2. CMA: Chaperone mediated autophagy
3. ROS: Reactive Oxygen Species
4. DIPEA: N,N-Diisopropylethylamine
5. DMF: N,N-Dimethylformamide
6. ESI-MS: Electrospray ionization – mass spectrometry
7. Fmoc: Fluorenylmethyloxycarbonyl
8. HATU: Bis(dimethylamino)methylene]-1H-1,2,3-triazolo[4,5-b]pyridinium-3-oxidhexafluoro phosphate
9. HBTU: Hexafluorophosphate Benzotriazole Tetramethyl Uronium
10. LCMS: Liquid chromatography
11. LC3: Light chain 3
12. ICT: Intramolecular/Internal Charge Transfer
13. LIR: LC3 – Interacting region
14. LRMS: Low resolution mass spectroscopy
15. NMR: Nuclear magnetic Resonance
16. TFA: Trifluoroacetic acid
17. DFT: Density functional theory
18. TD DFT: Time-dependent density-functional theory
19. TCA: Tricarboxylic acid
20. DNA: Deoxyribonucleic Acid
21. mTOR: Mammalian target of rapamycin
22. ATG4: Autophagy-related gene 4
23. ULK1: Unc-51 like autophagy activating kinase 1
24. MAPK: Mitogen-activated protein kinase
25. AMPK: AMP-activated protein kinase
26. Nrf2: Nuclear factor erythroid 2–related factor 2
27. P62: Ubiquitin-binding protein
28. HOMO: Highest Occupied Molecular Orbital
29. LUMO: Lowest Unoccupied Molecular Orbital
30. DMSO: Dimethyl Sulfoxide

Chapter 1: Introduction

1.1 Autophagy: An essential cellular process

Autophagy is a stress-responsive catabolic degradation mechanism in eukaryotes that enables nutrition recycling and the optimal maintenance of amino acid pools [1]. It is responsible for digesting improperly folded or undesired proteins and damaged cell organelles and is most active under amino acid deficiency or starvation. The term "autophagy," derived from the Greek for "self-eating," refers to how a cell recycles its elements for survival. There are three types of autophagy, each defined by how intracellular components are carried to the lysosome for degradation: chaperone-mediated autophagy (CMA), microautophagy, and macroautophagy, [1-4] (Fig 1).

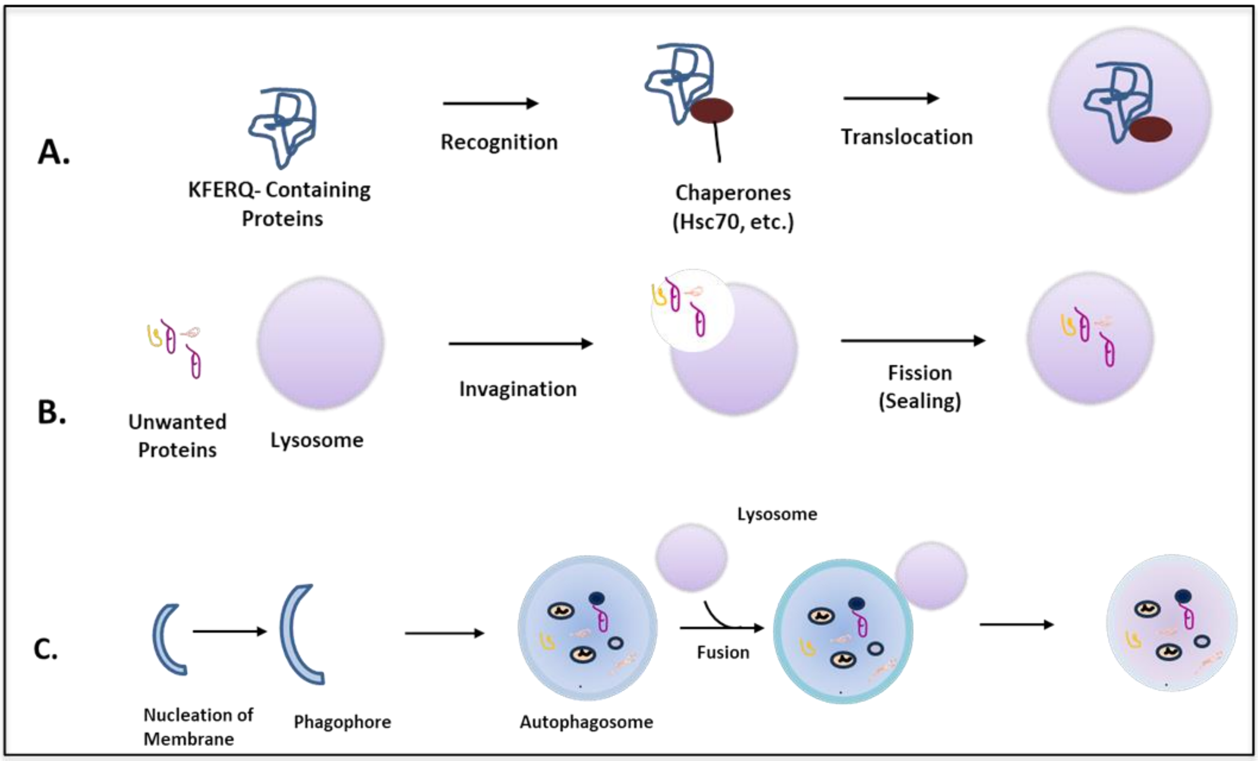

Fig. 1: Different types of autophagy: A. Chaperone-mediated autophagy, B. Microautophagy, C. Macroautophagy (Figure adapted from Reference 4)

a) **Chaperone-mediated autophagy** (CMA) is a selective process in which the Hsc70 chaperone recognizes proteins with a particular pentapeptide sequence (KFERQ-like) [1, 2, and 4]. These proteins are subsequently transported directly to lysosomes for breakdown. This process is different from the other autophagy types as it targets a specific pool of cytosolic proteins and uses a method to transfer substrate proteins to lysosomes. Approximately 30% of soluble cytosolic proteins are labeled with the KFERQ pentapeptide, which includes transcription factors, glycolytic enzymes, calcium-binding proteins, and vesicular traffickers. Only proteins with this targeting motif are identified by Hsc70 and transported to lysosomes [2].

b) **Microautophagy** sequesters cytoplasmic materials via direct invagination of the lysosomal membrane [4]. However, the molecular mechanism behind this action is still not entirely known.

c) **Macroautophagy**, the most prevalent type of autophagy, begins with the formation of autophagosomes, which are vesicles containing a double-membrane that encapsulate undesired proteins and damaged organelles for lysosomal degradation. This process can be selective, targeting specific cargoes such as mitochondria (mitophagy), or nonselective, happening in bulk under starvation. Impaired selective macroautophagy, such as mitophagy, is linked to various diseases. Other macroautophagy processes include ERphagy, Aggrephagy, Ribophagy, and Lipophagy [4]. This thesis focuses on macroautophagy, which shall be referred to simply as autophagy. Among the numerous autophagic processes, macroautophagy is the most common and intensively researched. As autophagy progresses, the proton concentration decreases due to lysosomal fusion [4], and variations in pH can be utilised as a strategy to distinguish between, as well as identify vesicles at various stages of autophagy.

1.2 Importance and Role of Autophagy

Autophagy, with its roles in nutrient recycling or anti-ageing, is essential for breaking down big protein aggregates, undesirable cell organelles, and invading microbes, including viruses, bacteria, and protozoa that proteasomes cannot trap. As a result, inhibiting or upregulating this mechanism may increase susceptibility to invading pathogens and disrupt cellular homeostasis, resulting in the onset of pathophysiological conditions like cancer, cardiovascular problems, and neurodegenerative ailments like Alzheimer's and Parkinson's [5]. Some of the physiological and pathophysiological roles of autophagy are mentioned below:

- **Amino acid pool maintenance**

The cellular amino acid pool is maintained by proteosomes, which break down cytoplasmic proteins. In order to preserve cellular homeostasis during nutritional shortage, autophagy preferentially breaks down proteins into amino acids. Although amino acids are not efficient energy sources, they are required for cellular function [6]. They have the potential to produce energy via the TCA cycle and gluconeogenesis during times of starvation [7]. Autophagy processes have been studied using model organisms such as *Saccharomyces cerevisiae*, *Dictyostelium discoideum*, Caenorhabditis elegans, *Drosophila melanogaster*, and mammalian cells [6, 8 and 9].

- **Intracellular quality control**

Autophagy maintains the amino acid pool not only under normal conditions, but also during starvation, until adequate nutrients are available in the system [6]. It maintains the intracellular amino acid concentration by constantly recycling cytoplasmic components. Deleting genes involved in autophagy causes malformed proteins and the buildup of undesired organelles. These misfolded proteins can cluster in the cytosol or intracellularly, causing considerable aggregation in a variety of organs including the liver, neurons, some endocrine glands, heart, and kidneys [6]. Basal autophagy, also known as constitutive autophagy, is especially important in the liver because of its rapid protein turnover, which is required for cellular equilibrium [6]. It is crucial in safeguarding neural tissues because it prevents protein aggregates from accumulating in nerve cell soma, which could otherwise injure the nerve cells [6, 10]. Neurodegenerative illnesses like Parkinson's, Alzheimer's, and polyglutamine (CAG) repeat diseases are characterized by the buildup of protein aggregates and autophagic vacuoles [6, 11, and 12]. Mutations in autophagy-related genes can cause aberrant proteins to accumulate in some familial neurodegenerative disorders [6]. As a result, autophagy is increasingly being viewed as a potential therapeutic target for a variety of neurodegenerative illnesses [6, 10].

- **Promotes growth and cell death**

Recent research has identified autophagy as an essential process that promotes growth in numerous organisms. Autophagy is often referred to as autophagic or type II cell death [6]. Some research suggests a link between autophagy and apoptosis. For instance, autophagy can induce cell death in cells lacking the ability to undergo apoptosis. Furthermore, cells undergoing apoptosis release phosphatidylserine (PS), a hallmark of old cells, allowing phagocytes to recognize and eliminate them. However, in cells without autophagy, PS is not exposed to the cell membrane due to a lack of ATP, resulting in the accumulation of cell debris and disturbing cellular homeostasis [6, 13].

- **Tumor suppression and cancer**

Autophagy is often initiated by starvation, a mechanism that also affects tumor cells, promoting their multiplication and contributing to cancer formation [6, 14]. Autophagy, conversely, can inhibit tumor proliferation by inducing cell death, removing sources of oxidative stress (such as faulty cell organelles that can cause DNA damage), or negatively regulating cell growth. When tumor cells are exposed to metabolic stress, this can prevent them from dying by apoptosis [6, 14].

- **Anti-aging and longevity**

Reactive oxygen species (ROS), most notably hydrogen peroxide, can be produced more frequently when defective organelles and incorrectly folded proteins accumulate, expediting the ageing of cells. Autophagy recycles ROS in cells, preventing their accumulation and earning it the term "anti-ageing process" [6, 14, and 15]. Autophagy's anti-ageing function prolongs cell longevity. As cells age, the concentration of damaged proteins rises due to decreased autophagy activity, resulting in a drop in metabolic function. As a result, autophagy has been identified as a possible therapeutic target for cellular ageing [14, 15].

- **Other human diseases**

Autophagy is frequently disrupted in a variety of human disorders, making it a possible marker for conditions such as neurodegeneration, myopathies, liver and heart disorders, and some bacterial, fungal, and viral infections [16].

1.3 Interplay Between ROS and Autophagy

Examples of reactive oxygen species (ROS) include molecules such as superoxide anion ($O2^{\bullet-}$), hydroxyl radical ($OH^{\bullet}$), and hydrogen peroxide (H_2O_2). These molecules play a crucial role in signaling at low concentrations and are produced by oxygen metabolism within cells [17]. However, in case of oxidative stress ROS can also be a factor, defined by high intracellular ROS concentrations that harm DNA, lipids, and proteins [18]. When oxidative phosphorylation occurs in healthy cells, electrons from the electron transport chain leak out of the mitochondria, producing most of the intracellular ROS [19, 20].

By focusing on genes like ATG4, transcription factors like HIF-1α, and signal transduction systems like mTOR and MAPKs, ROS control autophagy [33]. This regulation takes place through a variety of processes, including the oxidation of ATG4, which causes autophagosome formation, and the activation of AMPK by ROS, which causes phosphorylation of the ULK1 complex and promotes autophagy induction [32]. Conversely, autophagy helps lower ROS levels by eliminating damaged mitochondria (also known as mitophagy) or peroxisomes (pexophagy) [32]. Furthermore, in response to high levels of ROS, Nrf2 is activated from the nucleus, which stimulates the transcription of antioxidant genes [33]. This mechanism contributes to the restoration of ROS levels to equilibrium, emphasizing the complex balance between ROS and autophagy in cellular homeostasis [33].

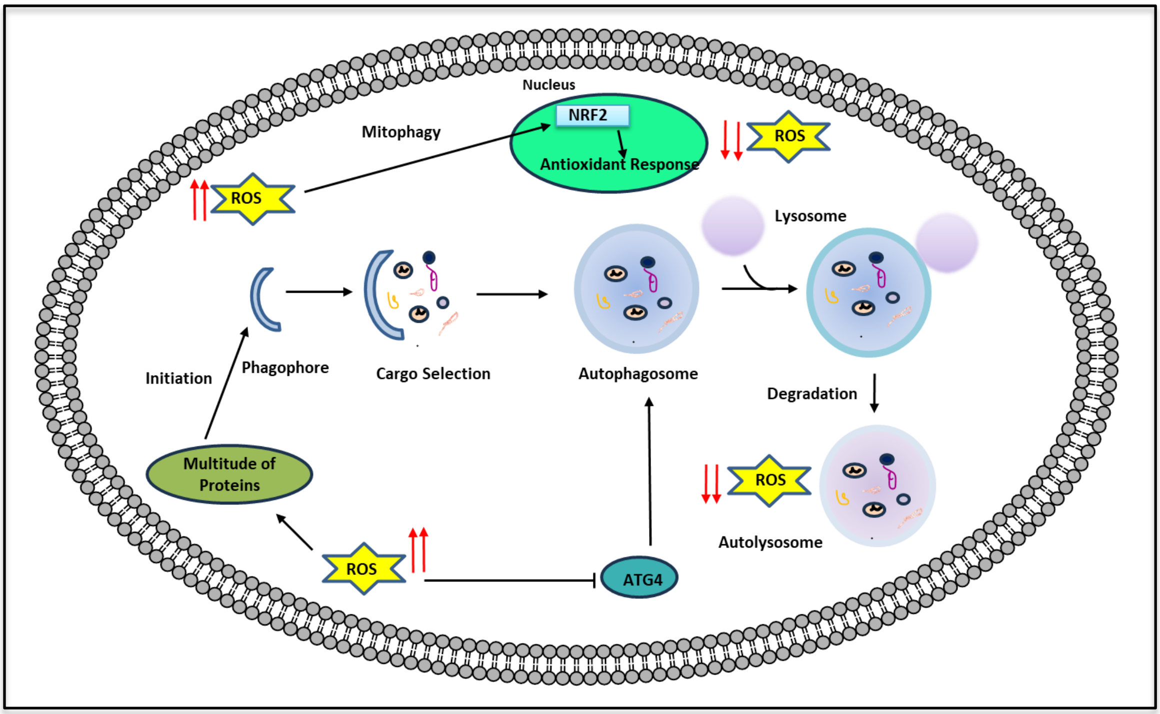

Fig. 2: Deciphering the Role of Reactive Oxygen Species (ROS) in Autophagy Regulation (Adapted from Ref. 33)

Among reactive oxygen species (ROS), hydrogen peroxide is distinguished by its extended half-life and low reactivity, which enable it to permeate through membranes and function as a signaling molecule in different cellular compartments [21, 22]. It functions as a second messenger and is essential for various cellular processes, including migration, differentiation, development, and proliferation [23-26]. Owing to its significance, the concentration of hydrogen peroxide is strictly controlled; any deviation from this might have negative consequences and exacerbate conditions including cancer, diabetes, heart disease, and neurodegeneration [27-31]. Thus, techniques for measuring hydrogen peroxide levels in living cells—especially in specialized compartments are to be developed in order to support biological research and aid in the early detection of disease. The following chapters 2 and 3 will describe the design and development of a sensor for detecting endogenous hydrogen peroxide in autophagic vesicles. Currently, we lack understanding of the specific variations in H_2O_2 levels at various stages of autophagy. Developing a sensor capable of monitoring H_2O_2 levels during the various stages of autophagy would be immensely beneficial. This sensor could not only provide information about dynamic changes in H_2O_2 concentrations, but it could also shed light on how H_2O_2 affects autophagic flux. Such a novel method would significantly improve our understanding of autophagy's role in various pathophysiological conditions.

ROS generation in Mitochondria

Often referred to as the "powerhouses of the cell," mitochondria are dynamic organelles that play a major role in regulating metabolism, producing energy within cells, and cellular fate and function [34]. The provided diagram depicts the generation of ROS within the mitochondria during the oxidative phosphorylation process (Fig. 3). Within the electron transport system, various redox complexes are present, and when electrons leak from this system and interact with free oxygen molecules, it leads to the formation of the superoxide ion. This superoxide ion serves as the primary contributor to ROS production [35].

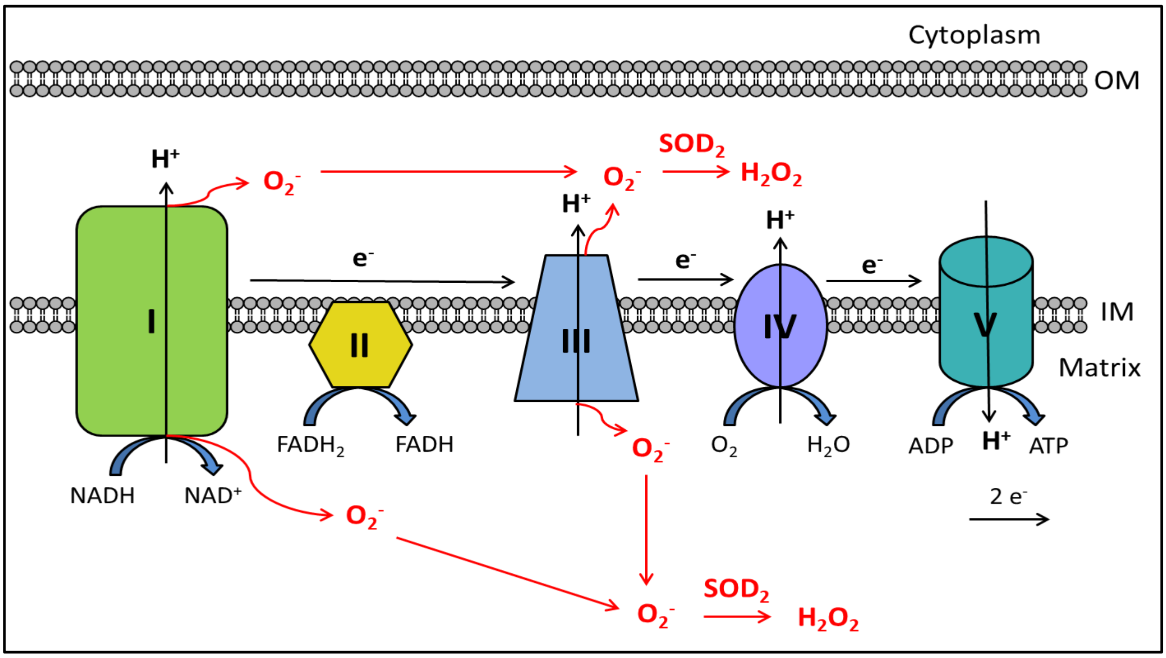

Fig. 3: ROS generation in Mitochondria during Oxidative Phosphorylation (Figure Adapted from Ref. 35)

1.5 The Interplay Between ROS and pH Dynamics in Mitochondria

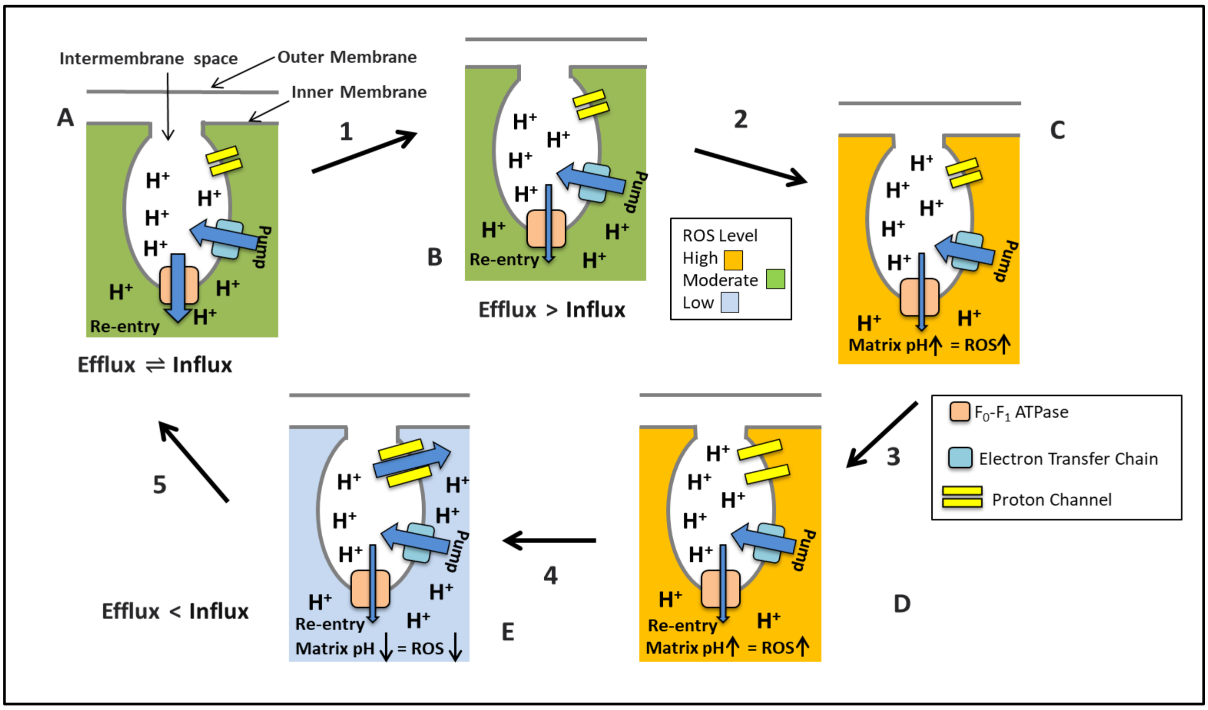

Fig. 4: The Interplay Between ROS and pH Dynamics in Mitochondria (Figure Adapted from Ref. 36)

The hypothesis presented in Fig. 15 suggests a sequence of events: (1) ROS generation is more likely when there is an increase in matrix pH due to an imbalance between proton influx and efflux (from State A, B to State C); (2) the elevated matrix pH triggers the opening of a proton channel (from State C to State D); (3) the resulting influx of protons lowers the matrix pH, reducing ROS production (from State D to State E); and (4) after the matrix pH decreases, [36].

The cited work proposes a relationship between spontaneous transient depolarization and ROS generation. Spontaneous brief depolarization may limit ROS generation within mitochondria by preventing a persistent rise of matrix pH [36]. Therefore, it is evident that there should be significant correlation between pH and ROS levels in mitochondria.

The last chapter, Chapter 4, an attempt has been made to synthesize sensors for monitoring the proton concentration and hydrogen peroxide levels within mitochondria toward elucidating the correlation between these two important analytes within this organelles.

References

1. Boya, P., Reggiori, F., & Codogno, P. (2013). Emerging regulation and functions of autophagy. Nature Cell Biology, 15(7), 713–720. https://doi.org/10.1038/ncb2788
2. Badadani, M. (2012). Autophagy Mechanism, Regulation, Functions, and Disorders. ISRN Cell Biology (Print), 2012, 1–11. https://doi.org/10.5402/2012/927064
3. Morel, É., Mehrpour, M., Botti, J., Dupont, N., Hamaï, A., Nascimbeni, A. C., & Codogno, P. (2017). Autophagy: a druggable process. Annual Review of Pharmacology and Toxicology, 57(1), 375–398. https://doi.org/10.1146/annurev-pharmtox-010716-104936
4. Mizushima, N., Levine, B., Cuervo, A. M., & Klionsky, D. J. (2008). Autophagy fights disease through cellular self-digestion. Nature, 451(7182), 1069–1075. https://doi.org/10.1038/nature06639

5. Levine, B., Mizushima, N., & Virgin, H. W. (2011). Autophagy in immunity and inflammation. Nature, 469(7330), 323–335. https://doi.org/10.1038/nature09782
6. Mizushima, N. (2009). Physiological functions of autophagy. Current Topics in Microbiology and Immunology, 335, 71–84. https://doi.org/10.1007/978-3-642-00302-8-3
7. Nofal, M., Zhang, K., Han, S., & Rabinowitz, J. D. (2017). MTOR inhibition restores amino acid balance in cells dependent on catabolism of extracellular protein. Molecular Cell, 67(6), 936-946.e5. https://doi.org/10.1016/j.molcel.2017.08.011
8. Kang, C., You, Y., & Avery, L. (2007). Dual roles of autophagy in the survival of Caenorhabditis elegans during starvation. Genes & Development, 21(17), 2161–2171. https://doi.org/10.1101/gad.1573107
9. Vabulas, R. M., & Hartl, F. U. (2005). Protein Synthesis upon Acute Nutrient Restriction Relies on Proteasome Function. Science, 310(5756), 1960–1963. https://doi.org/10.1126/science.1121925
10. Luo, Y., Fu, Y., Huang, Z., & Li, M. (2021). Transition metals and metal complexes in autophagy and diseases. Journal of Cellular Physiology, 236(10), 7144–7158. https://doi.org/10.1002/jcp.30359
11. Anglade, P., Vyas, S., Javoy-Agid, F., Herrero, M. T., Michel, P. P., Marquez, J., Mouatt-Prigent, A., Ruberg, M., Hirsch, E. C., & Agid, Y. (1997). Apoptosis and autophagy in nigral neurons of patients with Parkinson’s disease. Histology and Histopathology, 12(1), 25–31. https://pubmed.ncbi.nlm.nih.gov/9046040
12. Petersén A, A., Larsen, K. E., Behr, G. G., Romero, N., Przedborski, S., Brundin, P., & Sulzer, D. (2001). Brain-derived neurotrophic factor inhibits apoptosis and dopamine-induced free radical production in striatal neurons but does not prevent cell death. Brain Research Bulletin, 56(3–4), 331–335. https://doi.org/10.1016/s0361-9230(01)00580-9
13. Qu, X., Zou, Z., Sun, Q., Luby-Phelps, K., Cheng, P., Hogan, R. N., Gilpin, C., & Levine, B. (2007). Autophagy gene-dependent clearance of apoptotic cells during embryonic development. Cell, 128(5), 931–946. https://doi.org/10.1016/j.cell.2006.12.044

14. Hasan, A., Rizvi, S. F., Parveen, S., Pathak, N., Nazir, A., & Mir, S. S. (2022). Crosstalk Between ROS and Autophagy in Tumorigenesis: Understanding the Multifaceted Paradox. Frontiers in Oncology, 12, 852424. https://doi.org/10.3389/fonc.2022.852424.
15. Wang, X., Shi, W., Wang, K., Ye, Z., Wang, R., Wang, H., Yang, H., Xie, Z., Yu, H., & Wang, Y. (2023). Rationally Designed Nonapeptides with Great Skin Photoprotective Effect through Producing Type 1 Collagen and Blocking the mTOR Pathway. Journal of Medicinal Chemistry, 66(11), 7615–7628. https://doi.org/10.1021/acs.jmedchem.3c00503.
16. Mizushima, N. (2018). A brief history of autophagy from cell biology to physiology and disease. Nature Cell Biology, 20(5), 521–527. https://doi.org/10.1038/s41556-018-0092-5
17. Gough, D. R., & Cotter, T. G. (2011). Hydrogen peroxide: a Jekyll and Hyde signalling molecule. Cell Death and Disease, 2(10), e213. https://doi.org/10.1038/cddis.2011.96
18. Cross, C. E., Halliwell, B., Borish, E. T., Pryor, W. A., Ames, B. N., Saul, R. L., McCord, J. M., & Harman, D. (1987). Oxygen radicals and human disease. Annals of Internal Medicine, 107(4), 526. https://doi.org/10.7326/0003-4819-107-4-526
19. St-Pierre, J., Buckingham, J. A., Roebuck, S. J., & Brand, M. D. (2002). Topology of Superoxide Production from Different Sites in the Mitochondrial Electron Transport Chain. Journal of Biological Chemistry, 277(47), 44784–44790. https://doi.org/10.1074/jbc.m207217200
20. Murphy, M. P. (2008). How mitochondria produce reactive oxygen species. Biochemical Journal, 417(1), 1–13. https://doi.org/10.1042/bj20081386
21. Funato, Y., Michiue, T., Asashima, M., & Miki, H. (2006). The thioredoxin-related redox-regulating protein nucleoredoxin inhibits Wnt–β-catenin signalling through Dishevelled. Nature Cell Biology, 8(5), 501–508. https://doi.org/10.1038/ncb1405
22. Rhee, S. G. (2006). H 2 O 2 , a necessary evil for cell signaling. Science, 312(5782), 1882–1883. https://doi.org/10.1126/science.1130481
23. Kamata, H., Honda, S., Maeda, S., Chang, L., Hirata, H., & Karin, M. (2005). Reactive oxygen species promote TNFA-Induced death and sustained JNK

activation by inhibiting MAP kinase phosphatases. Cell, 120(5), 649–661. https://doi.org/10.1016/j.cell.2004.12.041

24. Finkel, T., & Holbrook, N. J. (2000). Oxidants, oxidative stress and the biology of ageing. Nature, 408(6809), 239–247. https://doi.org/10.1038/35041687
25. Winterbourn, C. C. (2008). Reconciling the chemistry and biology of reactive oxygen species. Nature Chemical Biology, 4(5), 278–286. https://doi.org/10.1038/nchembio.85
26. Ray, P. D., Huang, B., & Tsuji, Y. (2012). Reactive oxygen species (ROS) homeostasis and redox regulation in cellular signaling. Cellular Signalling, 24(5), 981–990. https://doi.org/10.1016/j.cellsig.2012.01.008
27. Mattson, M. P. (2004). Pathways towards and away from Alzheimer’s disease. Nature, 430(7000), 631–639. https://doi.org/10.1038/nature02621
28. Barnham, K. J., Masters, C. L., & Bush, A. I. (2004). Neurodegenerative diseases and oxidative stress. Nature Reviews Drug Discovery, 3(3), 205–214. https://doi.org/10.1038/nrd1330
29. Houstis, N. E., Rosen, E. D., & Lander, E. S. (2006). Reactive oxygen species have a causal role in multiple forms of insulin resistance. Nature, 440(7086), 944–948. https://doi.org/10.1038/nature04634
30. Ishikawa, K., Takenaga, K., Akimoto, M., Koshikawa, N., Yamaguchi, A., Imanishi, H., Nakada, K., Honma, Y., & Hayashi, J. (2008). ROS-Generating mitochondrial DNA mutations can regulate tumor cell metastasis. Science, 320(5876), 661–664. https://doi.org/10.1126/science.1156906
31. Xu, F., Li, H., Yao, Q., Fan, J., Wang, J., & Peng, X. (2016). A NIR fluorescent probe: imaging endogenous hydrogen peroxide during an autophagy process induced by rapamycin. Journal of Materials Chemistry B, 4(46), 7363–7367. https://doi.org/10.1039/c6tb02463g
32. Hasan, A., Rizvi, S. F., Parveen, S., Pathak, N., Nazir, A., & Mir, S. S. (2022c). Crosstalk between ROS and autophagy in tumorigenesis: Understanding the multifaceted paradox. Frontiers in Oncology, 12. https://doi.org/10.3389/fonc.2022.852424
33. Ornatowski, W., Lü, Q., Yegambaram, M., Garcia, A. E., Zemskov, E. A., Maltepe, E., Fineman, J. R., Wang, T., & Black, S. M. (2020). Complex interplay between autophagy and oxidative stress in the development of

pulmonary disease. Redox Biology, 36, 101679. https://doi.org/10.1016/j.redox.2020.101679

34. Alberts, B., Johnson, A., Lewis, J., Raff, M., Roberts, K., & Walter, P. (2002). Molecular Biology of the Cell. 4th edition. Garland Science.
35. Dikalov, S. (2011). Cross talk between mitochondria and NADPH oxidases. Free Radical Biology and Medicine, 51(7), 1289–1301. https://doi.org/10.1016/j.freeradbiomed.2011.06.033
36. Aklima, J., Onojima, T., Kimura, S., Umiuchi, K., Shibata, T., Kuraoka, Y., Oie, Y., Suganuma, Y., & Ohta, Y. (2021). Effects of matrix pH on spontaneous transient depolarization and reactive oxygen species production in mitochondria. Frontiers in Cell and Developmental Biology, 9. https://doi.org/10.3389/fcell.2021.692776

Chapter 2: Cell Permeable, Water Soluble, Peptide-based Fluorescent Sensor to Track the ROS and pH Levels in Autophagic Vesicles

2.1 Sensor Design

2.1.1 Introduction

Fluorescence microscopy is an effective and non-invasive technique for visualizing living cells and optically transparent organisms. High sensitivity and spatiotemporal resolution enable accurate imaging of cellular internal processes and signaling networks [1]. For example, the advancement of autophagy, a cellular degradation process, is associated with a drop in pH within autophagic compartments. The Datta group developed HCFP, a peptide-based, cell-permeable autophagy sensor to address the drawbacks of protein-based probes that are easily degraded [2]. This sensor also has the advantage of eliminating the need for transient transfection for sensor incorporation into living cells, as the sensor is cell-permeable [2].

Advancements in chemical techniques for detection of intracellular hydrogen peroxide (H_2O_2) have resulted in the creation of a diverse array of probes. Chang and colleagues synthesized several fluorescent probes [3], some of which can detect H_2O_2 in vitro and in vivo at physiological levels. These probes provide insights into the biological mechanisms linked to H_2O_2 [4, 5].

The bulk of these probes are fluorescent sensors [6, 7, 8] that increase in intensity when exposed to H_2O_2. However, interpreting the results of these turn-on probes can be difficult [9] because variations in the signal may not only show changes in H_2O_2 levels but can also be influenced by non-homogenous incorporation into cells. To address this issue, researchers developed ratiometric probes [10]. These probes produce fluorescence at various wavelengths both before and after reacting with H_2O_2. Because these probes generate fluorescence prior to H_2O_2 detection, it is easier to detect changes in intracellular probe concentration. Furthermore, the probe's fluorescence intensity ratio before and after H_2O_2 detection remains consistent regardless of probe concentration. This feature allows for more detailed and quantitative analysis [10].

However, molecular probes for ratiometric detection of H_2O_2 in autophagic vesicles have not been reported till now. In this chapter of the thesis, I have worked towards designing and developing a peptide-based ratiometric fluorescent sensor to track the H_2O_2 levels in autophagic vesicles. Additionally, a sensor for detecting autophagy that's labeled with a Rhodamine dye has been synthesized. The pH sensor is capable of distinguishing between vesicles at different stages of autophagy by measuring proton concentration levels within them. During autophagy, vesicles move from moderate to acidic pH conditions. With the progress of autophagy the pH within autophagic vesicles progressively decreases from 6.5 to 4.5. This rhodamine containing sensor can use the pH values to identify the stages of autophagy. Meanwhile, the ROS sensor detects reactive oxygen species levels, which fluctuate throughout autophagy, providing further information about the stage wise levels of hydrogen peroxide.

2.1.2 Design of the autophagosome targeted ROS sensor

As explained in Chapter 1 of the thesis, the drop in pH levels as autophagy advances emphasizes the need of determining H_2O_2 concentrations within different autophagic vesicles due to interlinked pathophysiological conditions. Thus, the development of an autophagosome-targeted pH probe and a similar ROS probe capable of detecting H_2O_2 is critical for understanding the dynamics of autophagy.

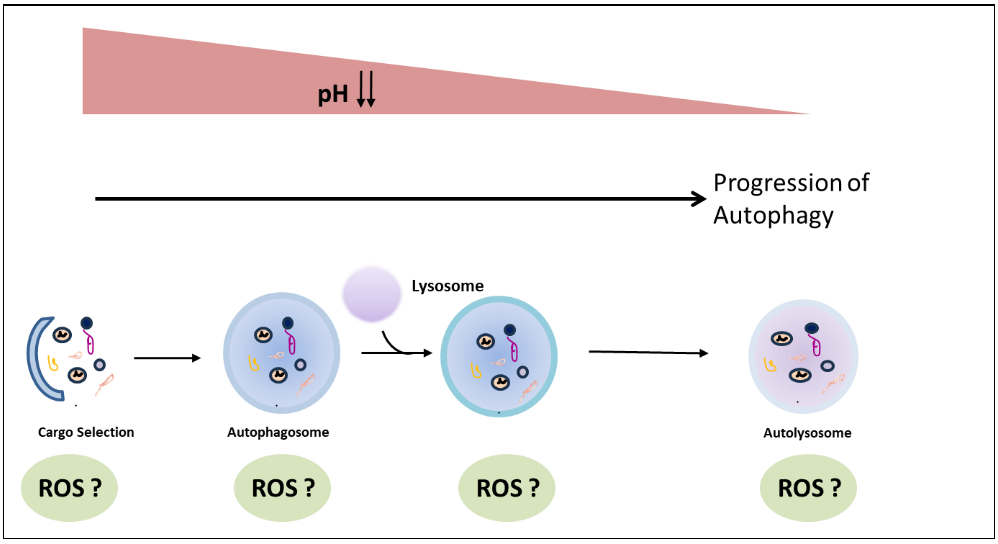

During autophagosome formation, the membrane closes, encapsulating cellular components for destruction. Two ubiquitin-like conjugates are required for this mechanism: the conjugate between ATG12 and ATG5, as well as the conjugation of phosphatidylethanolamine (PE) to ATG8 homologues like LC3 [11]. The ATG8-family interaction motif (AIM), required for selective autophagy, was first found in yeast and is conjugated to PE [12]. AIMs enhance the interaction of autophagy receptors and ATG-8 family proteins, aiding selective autophagy by connecting substrates to autophagosomal membranes.

ATG proteins consist of two domains: an initial helical domain at the N-terminus and a ubiquitin-like domain at the C-terminus. Among ATG-8 family proteins, only those possess dual α helices, designated as α1 and α2, at their N-terminal region. ATG-8 family proteins have exposed β-strands that bind AIM via an intermolecular β-sheet [12]. Atg8 has two hydrophobic pockets, the W-site between α2 and β2 and the L-site between β2 and α3, which interact with Tryptophan (W) and Leucine (L) residues in AIM, respectively [12].

Additionally, the p62/sequestosome facilitates the transfer of aggregated proteins to autophagic machinery by linking them to LC3, a mammalian analog of Atg8. This connection is made possible by the LC3 interacting region (LIR). Structures obtained through X-ray and NMR imaging of LC3 in conjunction with p62's LC3 interacting region (LIR) show that specific residues in p62's LC3 binding motif are critical for the interaction, implying that p62's WXXL sequence is a functional AIM required for LC3 binding. Molecular probes and modulators can precisely target autophagic vesicles using this consensus sequence [11, 13].

2.1.2 Selection of the autophagy targeting peptide sequence

Autophagy-related genes (ATGs) regulate the autophagy process. Cargo proteins like p62 assist in the delivery of improperly folded proteins and damaged organelles to the autophagic apparatus. These factors initially concentrate on autophagosomes. LC3-1 receptor proteins include a unique amino acid sequence known as the Atg-8 interaction motif (AIM), which interacts with Atg8 proteins on the autophagosome surface. Studies employing X-ray and NMR [12] have revealed that the consensus sequence for AIMs is Tryptophan-X-X-Leucine (WXXL), where X might be a hydrophobic or acidic residue. As a result, the peptide sequence was chosen based on the reported HCFP probe [2], with WTHL as the targeted sequence. To increase cell permeability, an arginine nonamer [14] was used. The target sequence was cleaved from the polyarginine using the GFLG amino acid sequence, which is cleavable by lysosomal proteases, such as Cathepsin B. a common cellular protease, cleaves this sequence, to ensure the presence of the probe in cytoplasm [2]. Since, the polyarginine tail is highly positively charged; this cleavage prevents the probe from accessing the nucleus. This strategy was employed to maintain the focus on observing autophagy, which primarily occurs within the cytoplasm [14].

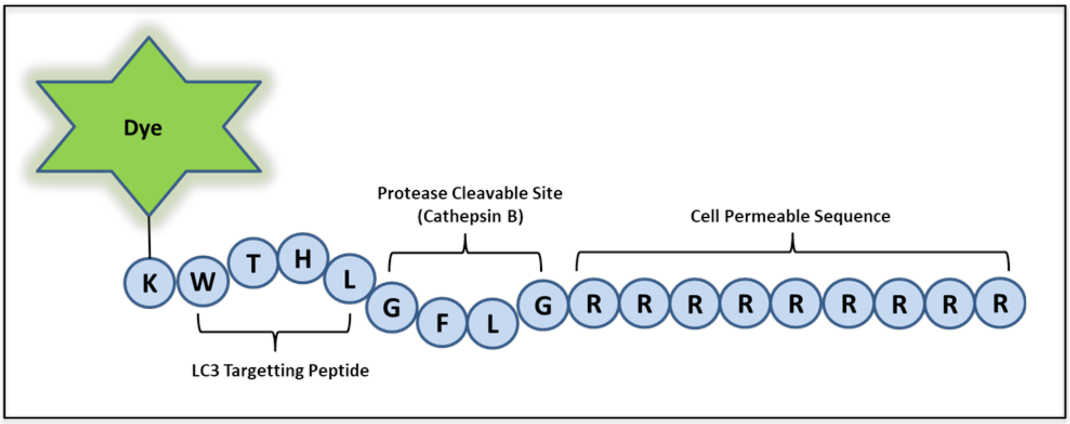

Fig. 5: Autophagy Peptide Design

Below are the designs of two autophagosome targeted probes for pH and ROS detection.

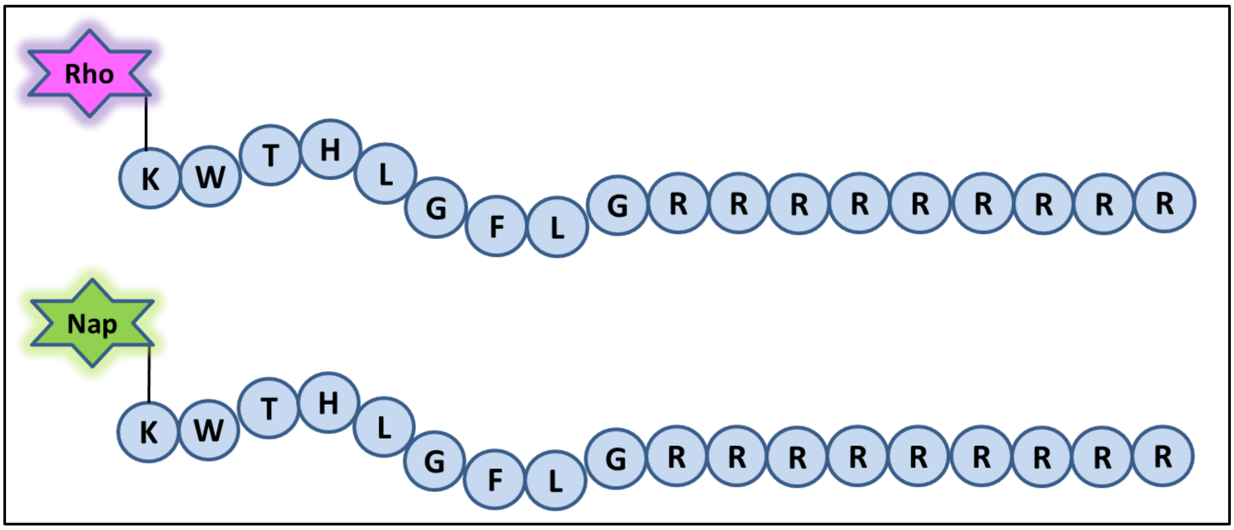

Fig. 6: Two Probe Designs, (a) Rho: Rhodamine, pH sensitive probe, (b) Nap: Napthalimide based ROS Probe

2.1.3 Selection of the napthalimide-based dye

There have been multiple reports using Intramolecular Charge Transfer based dyes with 1,8- Naphthalimide, a fluorescent chromophore and boric acid ester as the selective and sensitive hydrogen peroxide reporter [15, 16].

Since, the dye needs to be conjugated to an amino acid of the peptide via it's N-terminus, the dye needs to have a linker or a carboxylic acid arm to facilitate the process. The below figure describes the design and mechanism of action of the dye.

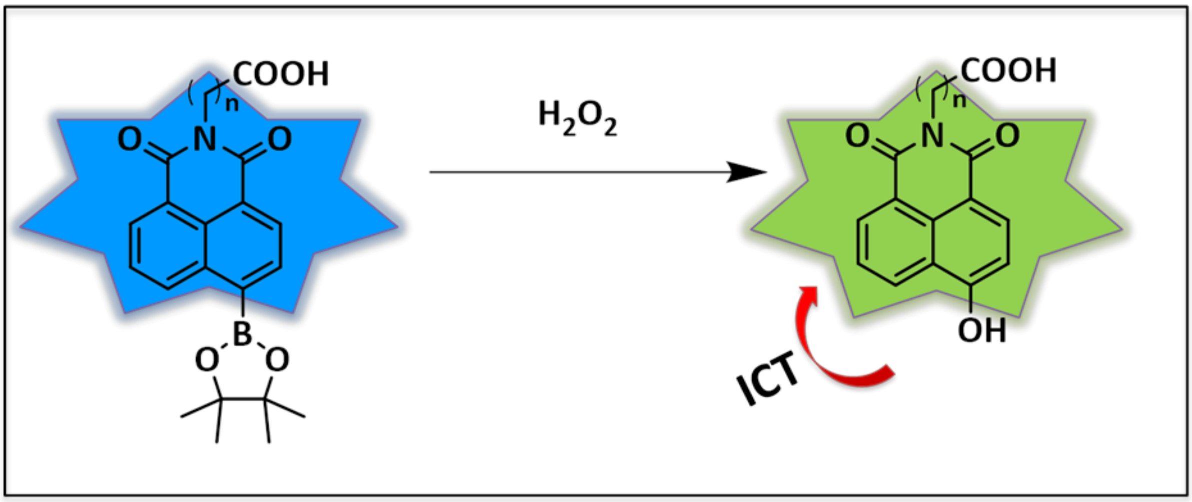

Fig. 7: Choice of the ROS Dye

2.1.3 Selection of the Rhodamine-based dye

Rhodamine spirolactone is commonly employed as a pH-sensitive structure in pH detection [25]. To connect the dye to an amino acid of the peptide via its N-terminus, a linker or carboxylic acid arm is required. Therefore, a dicarboxy version of Rhodamine is chosen for this purpose. When the lactone ring is hydrolyzed at a higher pH, the dye may exhibit a strong Stokes-shifted [26], turn-on response.

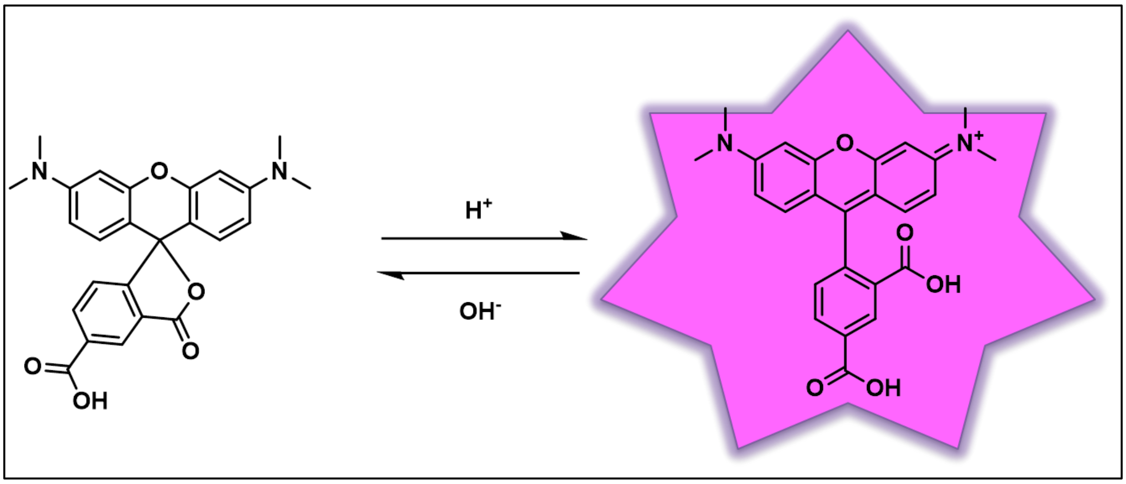

Fig. 8: Choice of the pH Dye

2.1.4 Final probe design

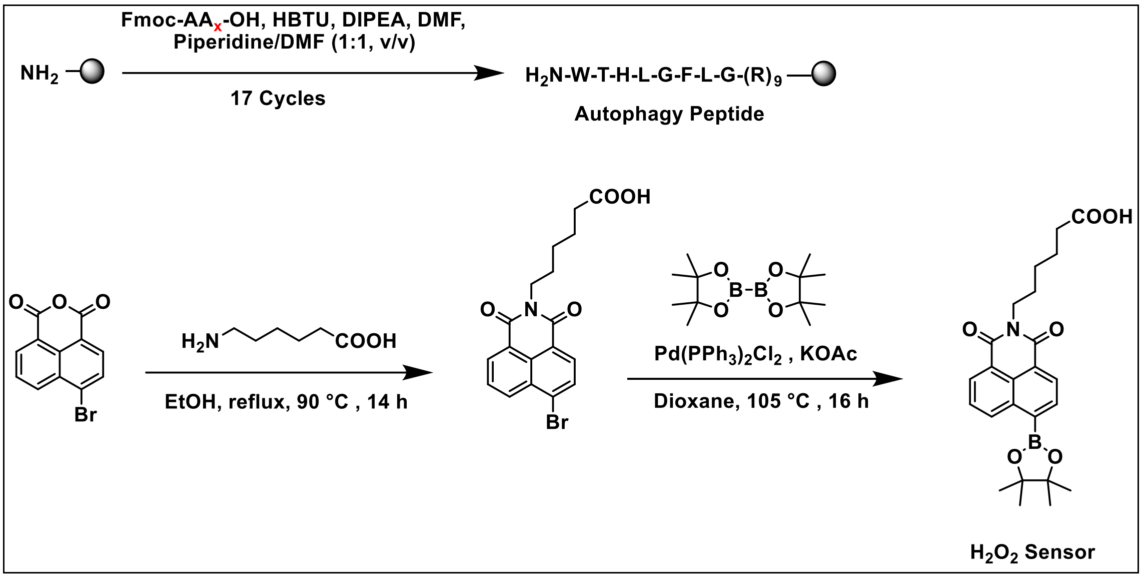

Fig. 9: Two Parts of the Probe

- **Synthetic Scheme for the ROS Probe (P1)**

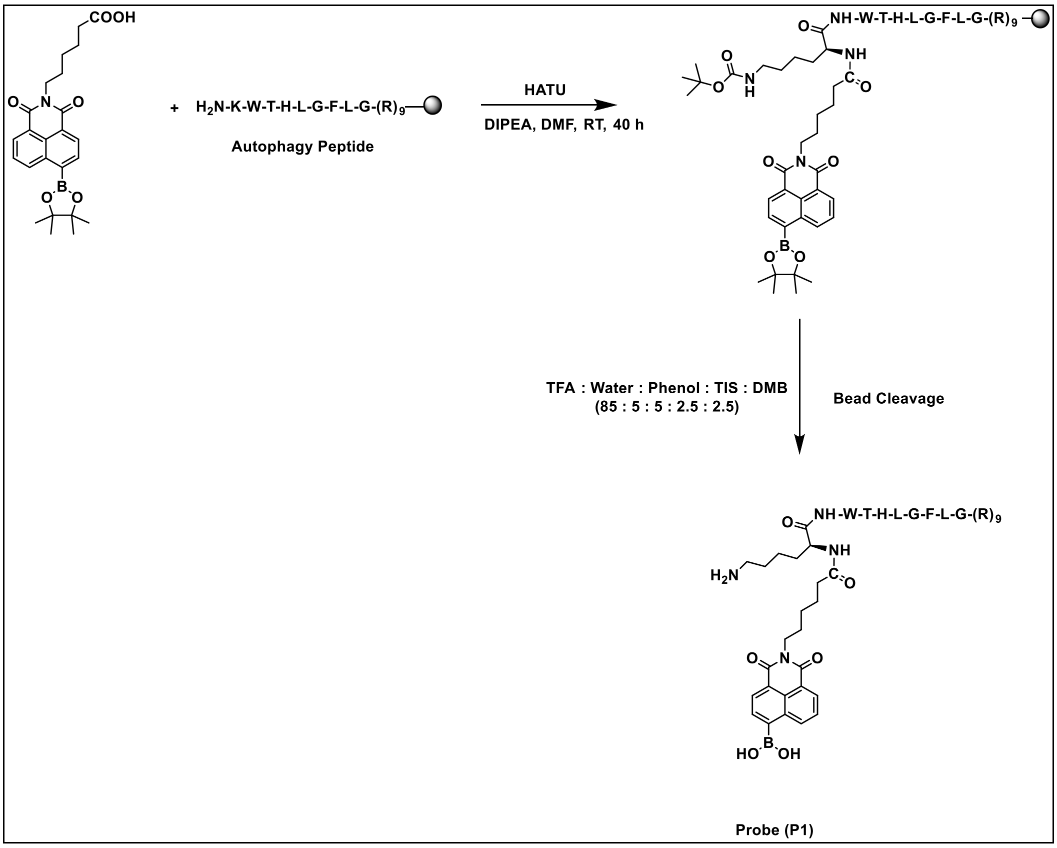

Fig. 10: Synthetic Scheme of the Probe (P1)

In this synthetic approach, the dye is directly attached to the Fmoc free N-terminus of the lysine containing autophagy targeted peptide utilizing a solid-phase synthesis method. Finally, the entire construct is cleaved from bead to yield the final probe (P1).

- **Synthetic Scheme for the pH Probe (P2)**

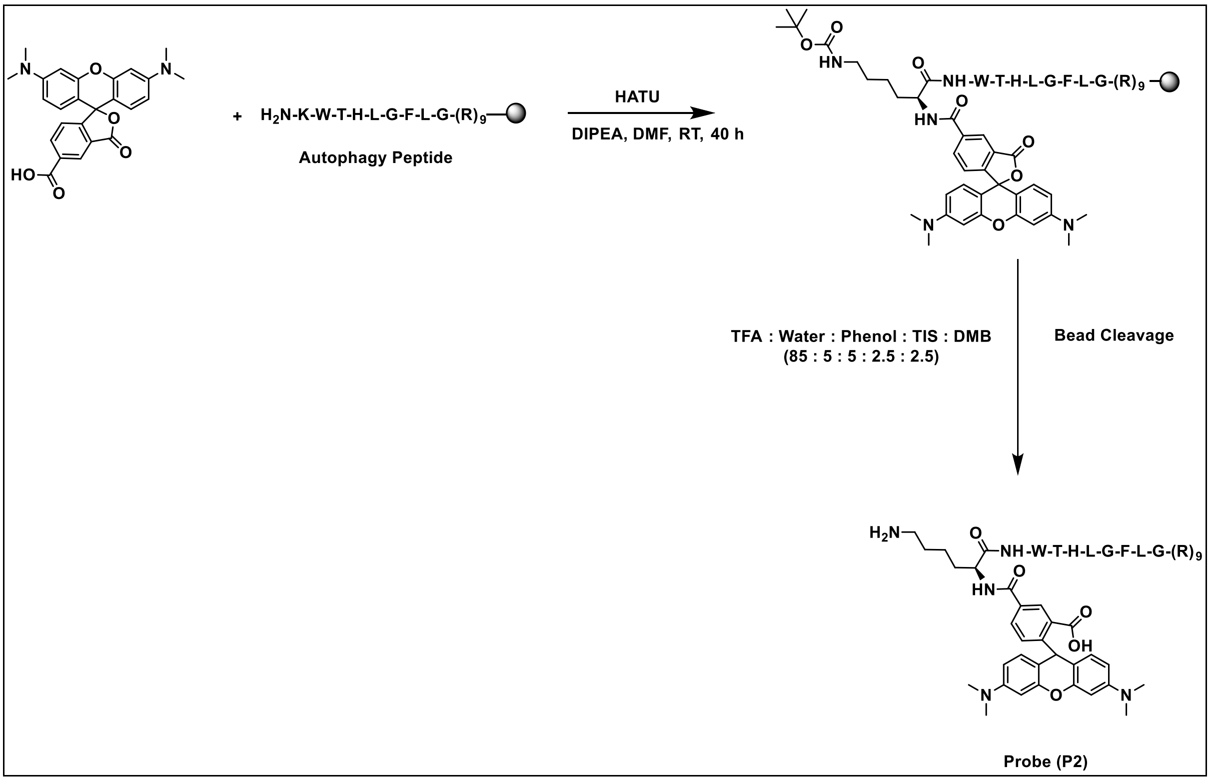

Fig. 11: Synthetic Scheme of the Probe (P2)

In this similar synthetic approach, the dye is directly attached to the Fmoc free N-terminus of the lysine containing autophagy targeted peptide utilizing a solid-phase synthesis method. Finally, the entire construct is cleaved from bead to yield the final probe (P2).

2.2 Materials

Unless otherwise mentioned, all chemicals used were of analytical grade, obtained from commercial sources and used without further purification. Solid-phase peptide synthesis resins were procured from Sigma Aldrich, and amino acids, and activating reagents used in peptide synthesis were procured from Novabiochem (Merck

Millipore). Other chemicals and solvents were purchased from either Sigma-Aldrich or Tokyo Chemical Industry (India) Private Limited and used without further purification. Water used for experiments was deionized using a Milli Q Integral 3 water purification unit (Millipore Corp. Billerica, MA, USA).

Low-resolution mass spectral analyses were carried out on a liquid chromatography-mass spectrometer (LCMS-2020, Shimadzu Corp.) with an ESI probe. Some peptide mass measurements were recorded on an Applied Biosystems 4800 Plus MALDI-TOF/TOF analyzer instrument using 1:1 α-Cyano-4-hydroxycinnamic acid (CHCA) and sinapinic acid (SA) matrix. ^{1}H NMR was collected in Deuterated Solvents at 25 °C on Varian 600 MHz spectrometers at the NMR facility, Tata Institute of Fundamental Research, Mumbai, India. All chemical shifts are reported in the standard notation of parts per million (ppm). Signals were internally referenced to solvent residual peaks. The abbreviations used for the proton spectra multiplicities are: s, singlet; br, broad; d, doublet; t, triplet; m, multiplet.

Fluorescence spectrum was recorded on Fluoromax®-3 (Horiba Jobin Yvon Inc.) spectrofluorometer using quartz cuvettes with 10 mm x 4 mm (Hellma® Analytics).

- **Solid Phase Peptide Synthesis Strategy**

The peptide was synthesised via solid phase peptide synthesis strategy on H-Rink amide ChemMatrix resin (35-100 mesh (wet sieved), loading 0.6 mmol/g resin) using a home built fast flow peptide synthesizer. A temperature of 60-70 °C was maintained during the synthesis by placing the reactor in a water bath set at the required temperature. The resin (100 mg, 0.06 mmol) was pre-swollen in DMF. Fmoc-protected amino acid (0.24 mmol), HBTU (92 mg, 0.24 mmol), and DIPEA (5 eq., 0.3 mmol) were added to a suspension of the resin in DMF (2 mL) and allowed to react for 10 min. This constituted the coupling step. Following the coupling step, the beads were washed with DMF and the Fmoc protection on the coupled amino acid was removed using 50% piperidine in DMF. The coupling steps with appropriate amino acids followed by the Fmoc deprotection step were repeated to afford the peptide on the Rink amide resin [2].

Next, TFA, TIS, DMB, water, and phenol (85: 2.5: 2.5: 5: 5) were added to the dried beads for the cleavage of the peptide from the bead. The beads were left in the cleavage mixture for 4 h. The mixture was filtered and the filtrate containing the desired compound was dried under Argon. Finally the crude cleaved peptide was precipitated out of cold diethyl ether and dried [2].

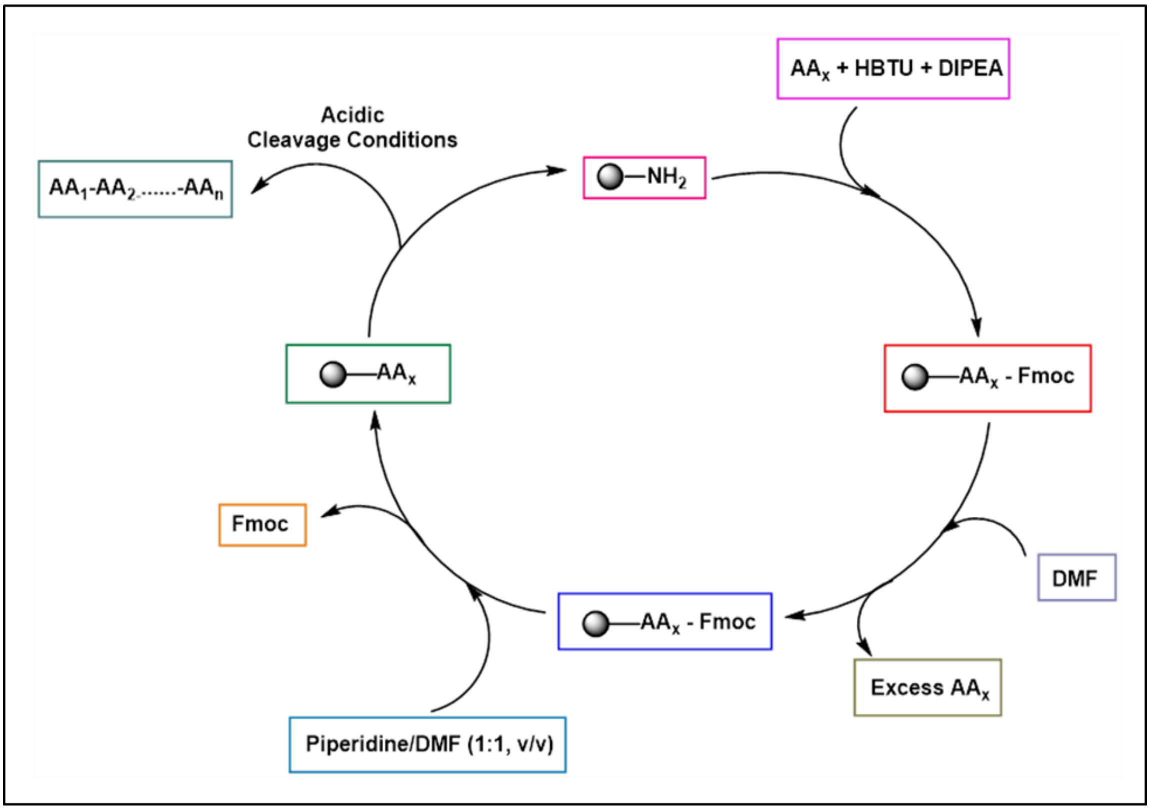

Fig. 12: Schematic Representation of Solid-Phase Peptide Synthesis

2.3 Methods

- **Synthesis of the H_2O_2 Probe**

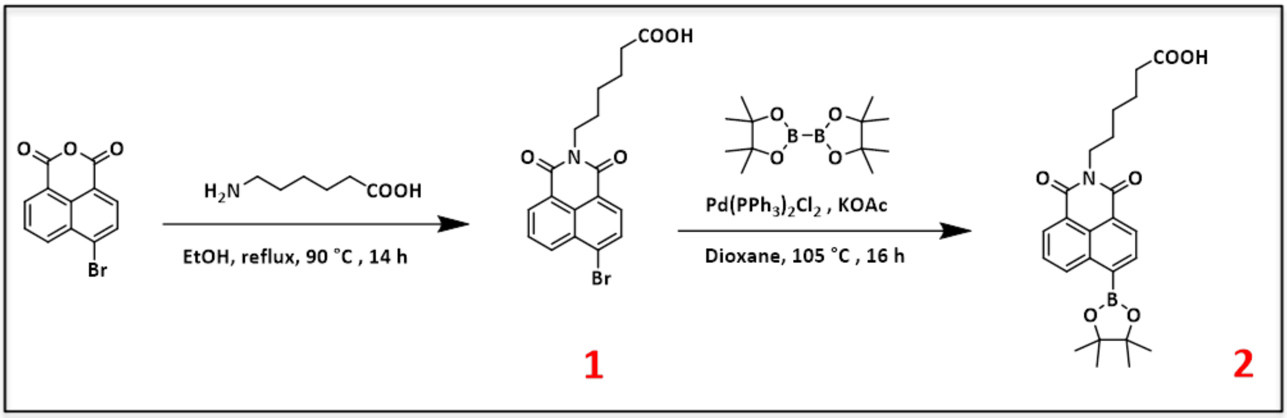

- **Synthesis of 1**

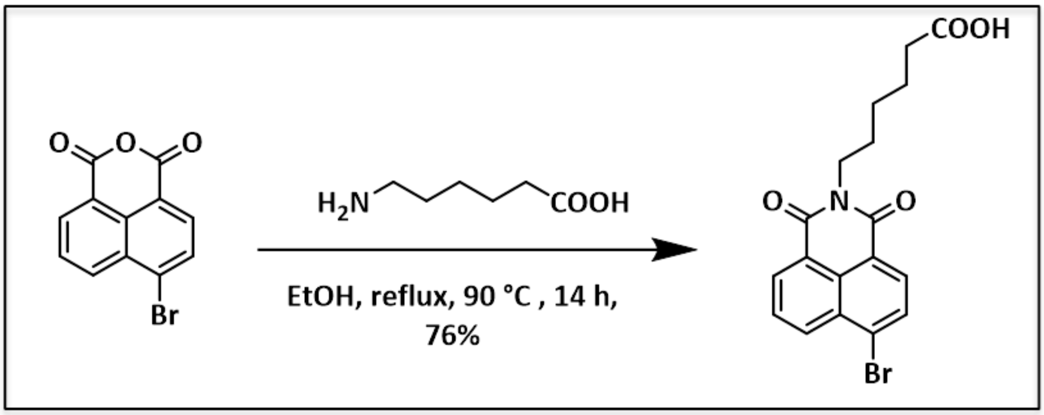

Procedure: 4-bromo-1,8-naphthalenedicarboxylic acid anhydride (500 mg, 1.8 mmol) and 6-aminocaproic acid (262 mg, 2.0 mmol) were dissolved in ethanol (40 mL) and refluxed at 90°C overnight. The reaction mixture was suction filtered while hot, filtrate recrystallization afforded light yellow solid (Yield = 76 %).

LRMS: m/z Calculated for M^+ = 389, Observed ($[M\text{-}H]^-$) = 388

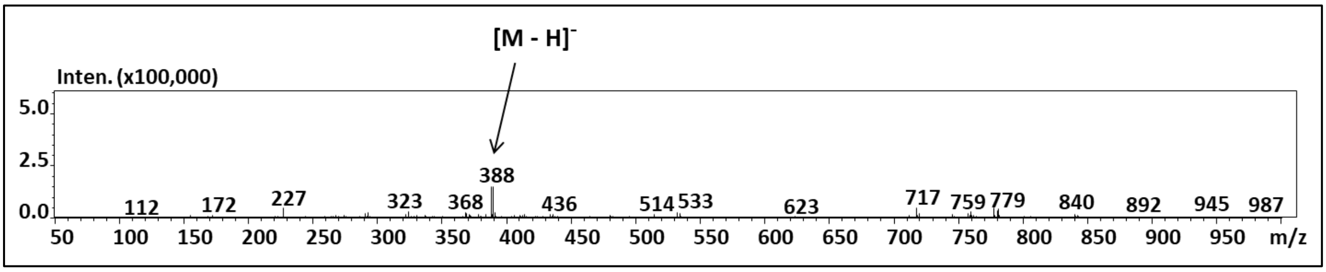

^{1}H NMR- (600 MHz, DMSO-d6) (ppm) 8.56 (d, J = 6.7 Hz, 1H), 8.54 (d, J = 8.4 Hz, 1H), 8.33 (d, J = 7.8 Hz, 1H), 8.21 (d, J = 7.9 Hz, 1H), 8.01 – 7.97 (m, 1H), 4.01 (t, J = 7.5 Hz, 2H), 2.20 (t, J = 7.3 Hz, 2H), 1.63 (t, J = 7.6 Hz, 2H), 1.56 – 1.52 (m, 2H), 1.34 (t, J = 7.8 Hz, 2H).

- **Synthesis of 2**

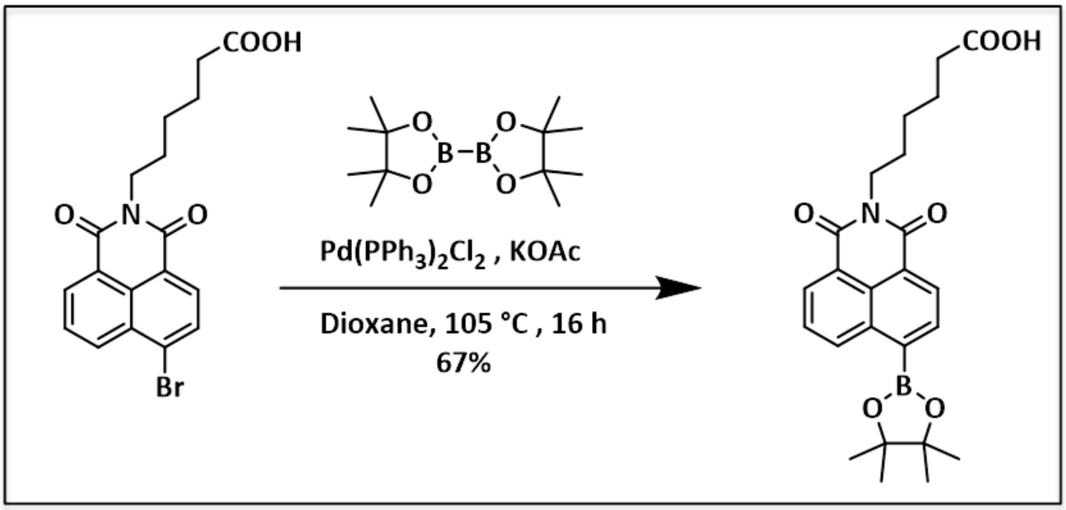

Procedure: At first, potassium acetate (175 mg, 1.785 mmol) was dried in vacuum, followed by the addition of dry, degassed 1,4-Dioxane (30 mL). Subsequently, $Pd(PPh_3)_2Cl_2$ (35.8 mg , 0.051 mmol) catalyst was introduced under a nitrogen atmosphere and 4-bromo-1,8-naphthalimide (200 mg, 0.51 mmol) was similarly added and the reaction setup was maintained at 60°C for a duration of 45 minutes under nitrogen atmosphere. In the final stage, bis(pinacolato)diboron (168 mg, 0.663 mmol) was introduced, and the reaction mixture was stirred at 105°C under reflux conditions overnight, under a nitrogen atmosphere. After cooling to room temperature, the solvent was evaporated under vacuum. The eluent of dichloromethane/methanol=80:1 (0.4% acetic acid) was passed through the silica column at to obtain a fluorescent small molecule, 67% yield.

LRMS: m/z Calculated for (M) = 437, Observed ($[M+H]^+$, $[M+Na]^+$, $[M+K]^+$,) = 438, 460, 476

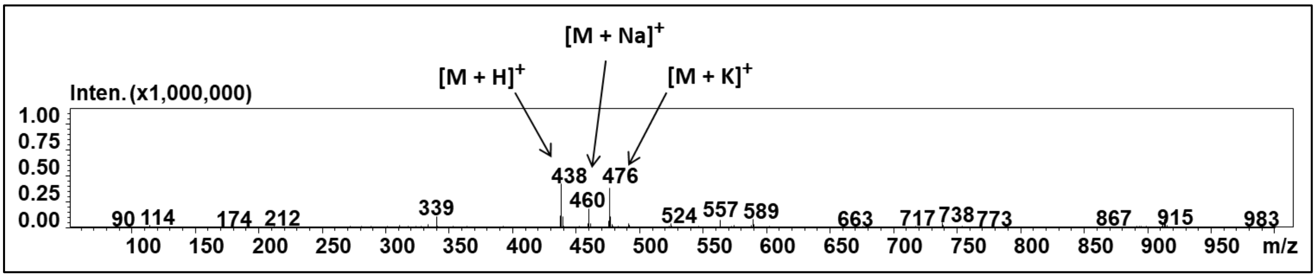

^{1}H NMR- (800 MHz, Chloroform-d) (ppm) 9.02 (d, J = 8.4 Hz, 1H), 8.48 (d, J = 7.2 Hz, 1H), 8.45 (d, J = 7.2 Hz, 1H), 8.20 (d, J = 7.2 Hz, 1H), 7.69 (t, J = 7.8 Hz, 1H), 4.12 (t, J = 7.6 Hz, 2H), 2.36 (t, J = 7.5 Hz, 2H), 1.72 (dt, J = 20.1, 7.7 Hz, 4H), 1.46 (t, J = 7.7 Hz, 2H), 1.42 (s, 12H).

^{13}C NMR- (200 MHz, Chloroform-d) (ppm) 177.19 , 164.35 , 135.78 , 135.00 , 130.92 , 129.82 , 127.89 , 127.10 , 122.58 , 84.61 , 40.19 , 33.52 , 27.69 , 26.54 , 24.99 , 24.42 .

- **Synthesis of the Autophagy Peptide**

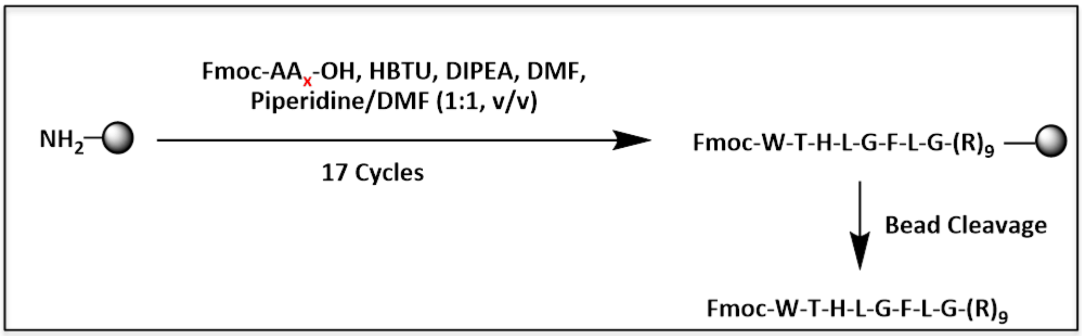

The peptide W-T-H-L-G-F-L-G-(R)9 was synthesized using solid state peptide synthesis method using Rink Amide Resin in our home-built fast flow peptide synthesizer based on the model developed by Prof. Bradley Pentelute and group [24]. The synthesis started by coupling the nine arginine residues first, followed by the rest of the amino acids on the rink amide resin bead. Once the entire Fmoc-containing peptide was synthesized the final compound was characterized using electrospray ionization mass spectrometry (ESI-MS), and MALDI-TOF.

MALDI-TOF: m/z Calculated for M^+ = 2557, Observed = 2557

LRMS: m/z Calculated for M^+ = 2334.80, Observed ($[M+2H]^{2+}/2$, $[M+3H]^{3+}/3$, $[M+4H]^{4+}/4$, $[M+5H]^{5+}/5$, = 1279, 853, 640, 512

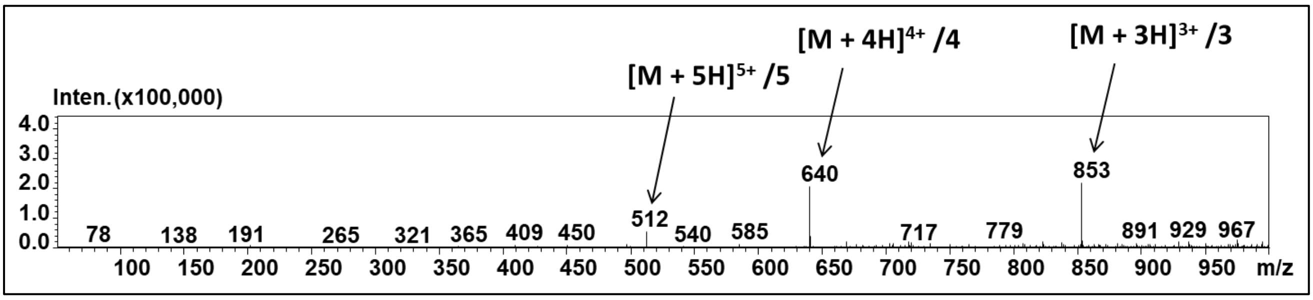

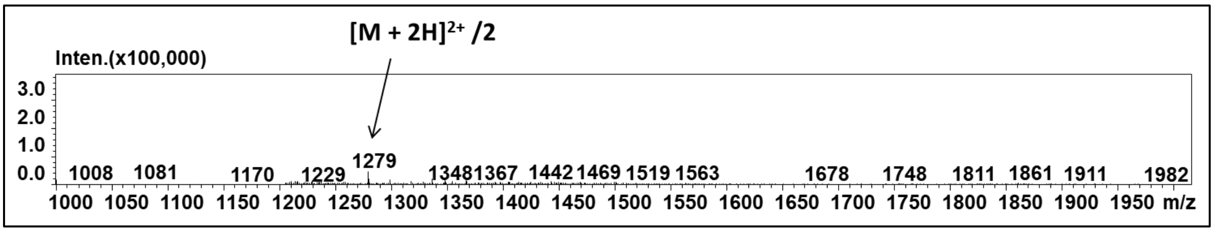

- **Synthesis of the Probe (P1)**

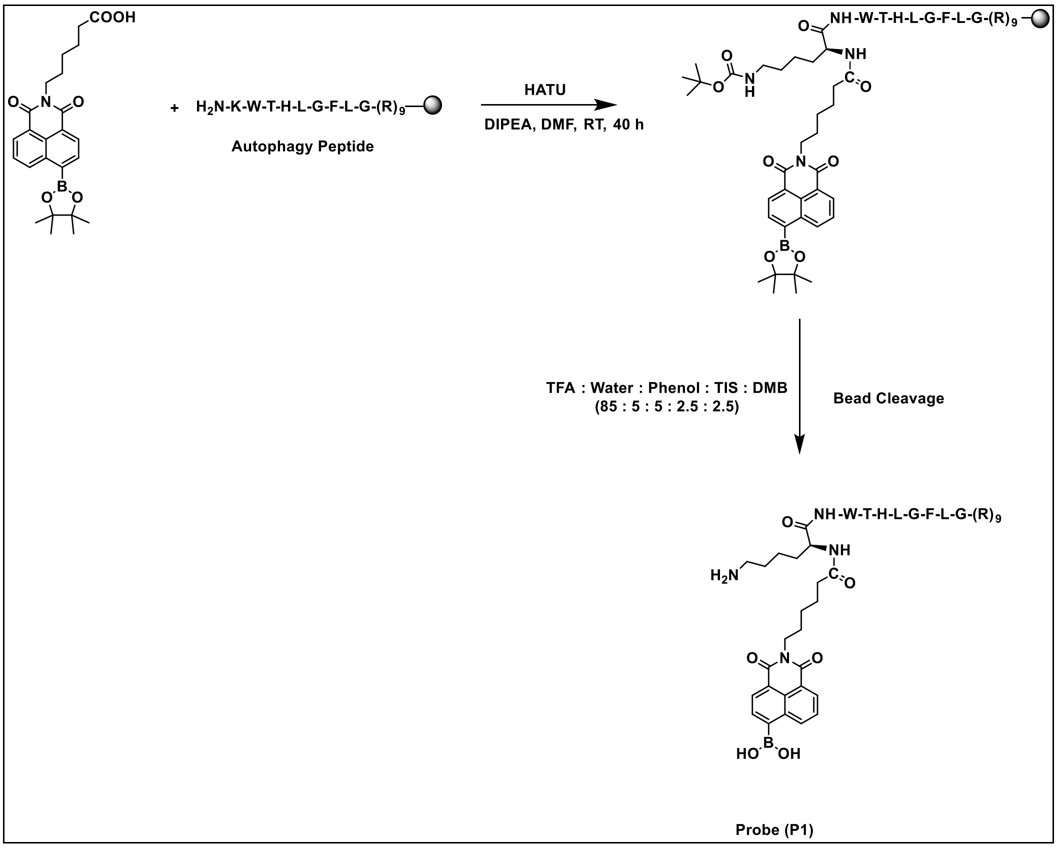

Procedure: The dye (2) molecule (7 mg, 0.0144 mmol) was dissolved in 1 mL of anhydrous DMF in an Eppendorf tube. DIPEA (11 µL, 0.0576 mmol) was then added to the solution, and the mixture was kept on a rotor for 15-30 minutes. Subsequently, HATU (22 mg, 0.0576 mmol) was added to the solution, and the reaction was allowed to proceed for an additional 15-30 minutes under rotor motion. Following this, Fmoc-free lysine-containing autophagy peptide beads (24 mg, 0.0144 mmol) were introduced into the reaction mixture, which was left to react for two days at room temperature on the rotor. The beads were then meticulously washed multiple times with DMF and methanol to eliminate any unreacted soluble organic components. The probe (P1) was obtained by cleaving the dried beads for two hours using the previously described method. The resulting precipitate was dried using a vacuum concentrator.

HRMS: m/z Calculated for M^+ = 2799, Observed ($[M+6H]^{6+}/6$, $[M+7H]^{7+}/7$) = 467.6107, 400.9535

- **Synthesis of the Probe (P2)**

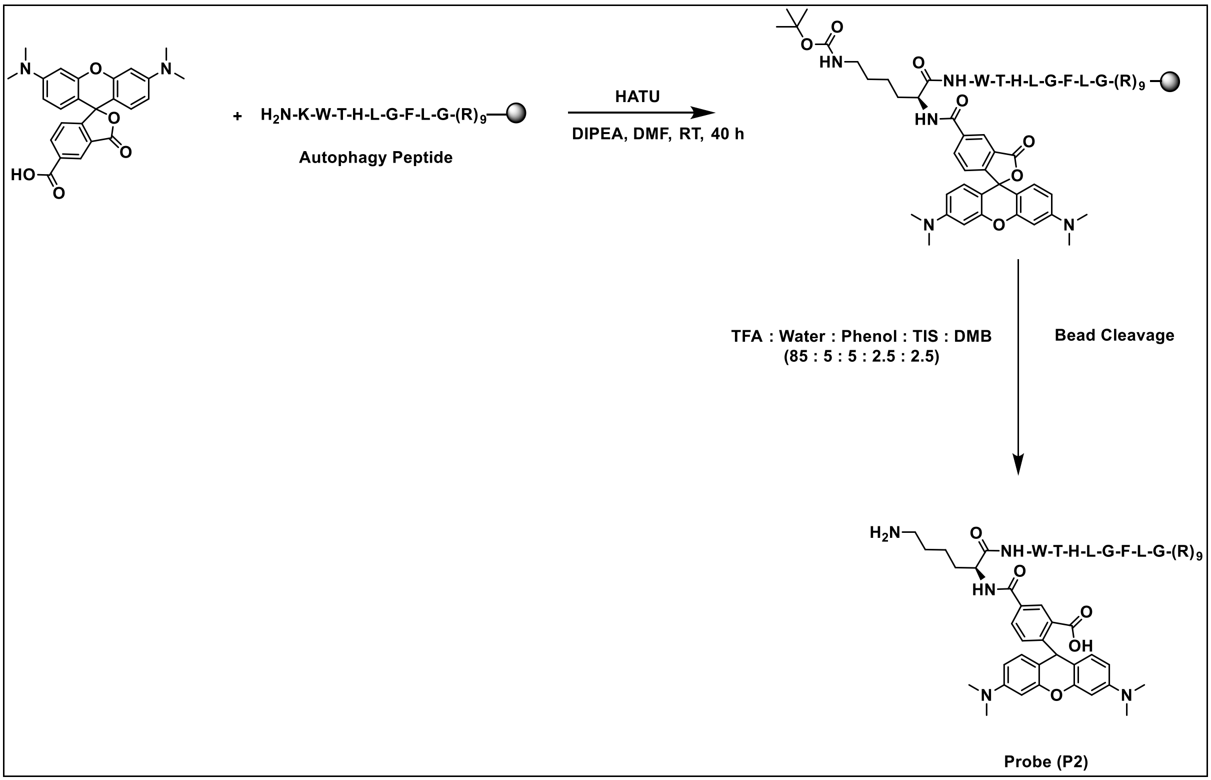

Procedure: 5-Carboxytetramethylrhodamine (5 mg, 0.0101 mmol) was dissolved in 1 mL of anhydrous DMF in an Eppendorf tube. DIPEA (11 µL, 0.0576 mmol) was then added to the solution, and the mixture was kept on a rotor for 15-30 minutes. Subsequently, HATU (22 mg, 0.0576 mmol) was added to the solution, and the reaction was allowed to proceed for an additional 15-30 minutes under rotor motion. Following this, Fmoc-free lysine-containing autophagy peptide beads (24 mg, 0.0144 mmol) were introduced into the reaction mixture, which was left to react for two days at room temperature on the rotor. The beads were then meticulously washed multiple times with DMF and methanol to eliminate any unreacted soluble organic components. The probe (P2) was obtained by cleaving the dried beads for fours hours using the previously described method. The resulting precipitate was dried using a vacuum concentrator.

LRMS: m/z Calculated for M^+ = 2874, Observed ($[M+2H]^+/2$, $[M+3H]^+/3$, $[M+5H]^{5+}/5$, $[M+6H]^{6+}/6$, $[M+7H]^{7+}/7$) = 959, 576, 480, 412

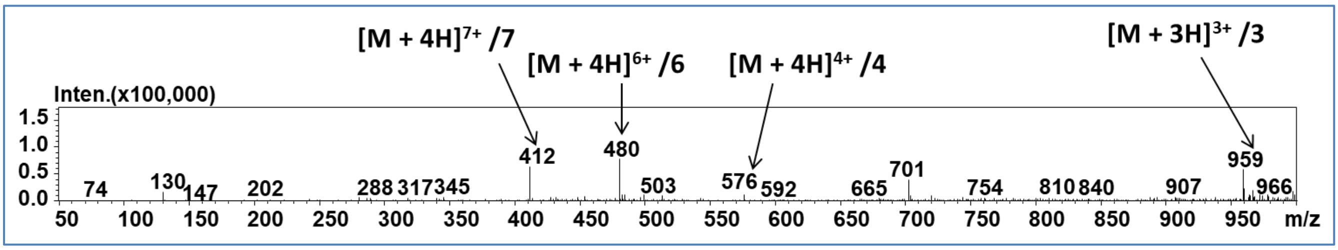

2.4 Results and Discussion

- **Purification of the Rhodamine Attached Peptide Probe**

The rhodamine attached peptide (Probe P2) was purified on a Varian PrepStar, SD-1 HPLC system, equipped with a Phenomenex Luna® C18(2) (250 x 10 mm) semi-preparative column. Acetonitrile and water with 0.1 % trifluoroacetic acid were used as mobile phase and absorption at 226 nm, 250 and 550 nm were monitored for product elution.

Solvent: Solvent A: Water with 0.1% trifluoroacetic acid; solvent B: Acetonitrile with 0.1%Trifluoroacetic acid.

Gradient: 0-5 min: 5% solvent B; 5-50 min: 5-100 % solvent B; 55 min: 100% solvent B; 60 min: 5% solvent B; 65 min: 5% solvent B. HPLC fractions were characterized by ESI-MS to identify fractions containing the desired product. Pure fractions were evaporated under reduced pressure in a vacuum concentrator, (Eppendorf Concentrator Plus, Eppendorf AG, Germany). Purity of the fractions was further confirmed by electro-spray ionization liquid chromatography mass spectroscopy (ESI-LCMS) (LCMS-2020, Shimadzu Corp.) equipped with a Phenomenex Luna® C18(2) column (150 x 4.6 mm) using acetonitrile and water with 0.1% trifluoroacetic acid as the mobile phase. Gradient: 5% solvent B (0-5 min), 5-100 % solvent B (5-40 min), 100% solvent B (40-60 min).

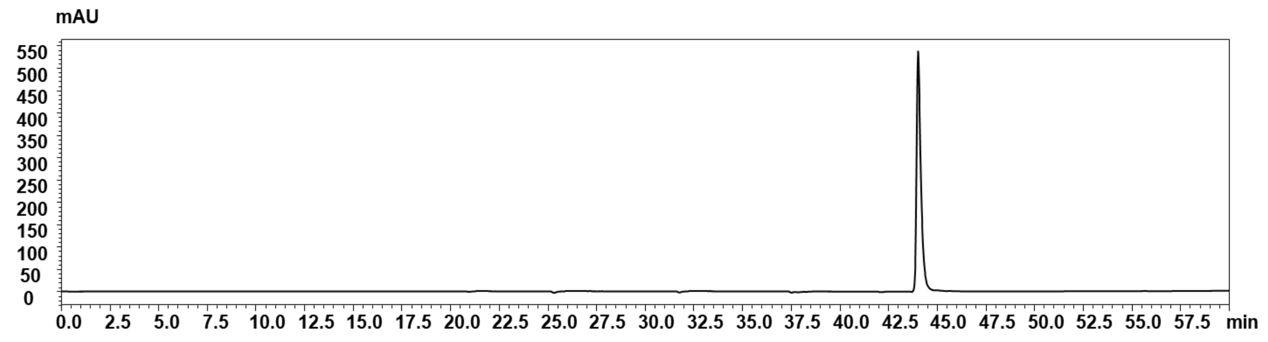

Fig. 13: LCMS trace for Probe P2 confirming sample purity. LC trace depicting absorption intensity at 550 nm

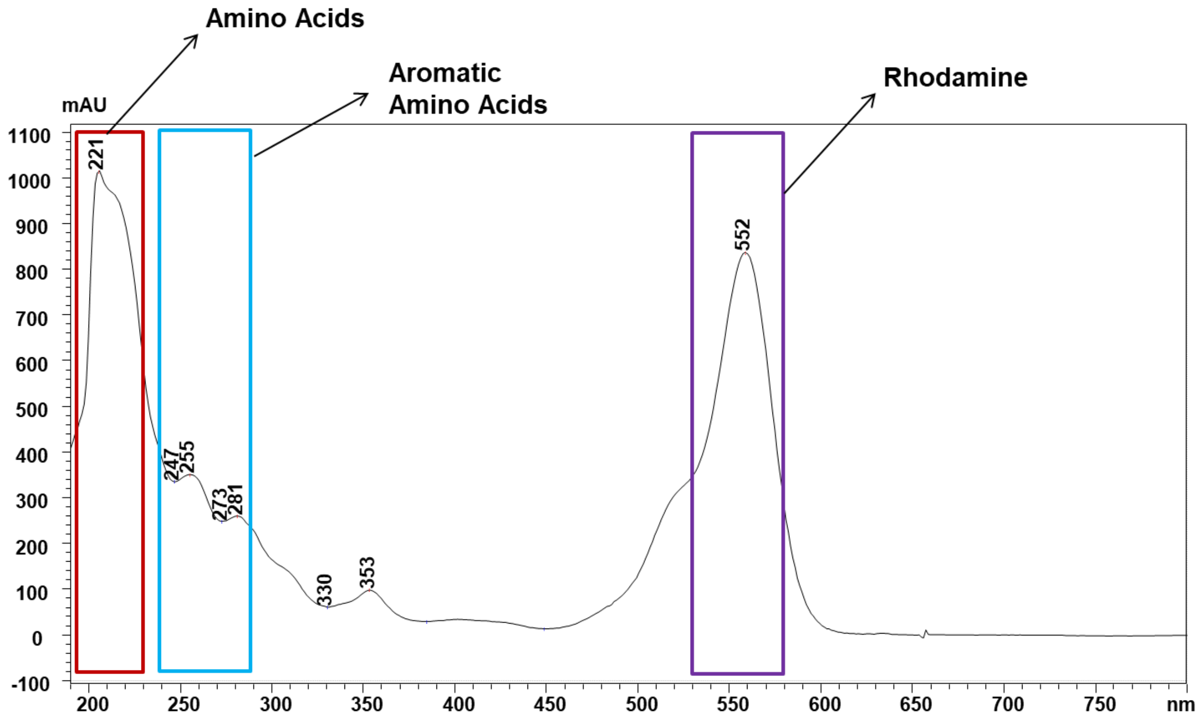

Fig. 14: Photodiode Array Detector (PDA) Absorbance Profile of the Purified Probe P2 after LC

- **In-Vitro Study of the Probe P2**

The experiments were conducted using the water-soluble probe (P2) in a 20 mM Na-HEPES, 20 mM NaCl aqueous buffer at pH 7.5 and room temperature. The probe, at a concentration of 1 µM and a volume of 200 µL, was excited at 525 nm. As the pH of the buffer was increased from 3 to 10, the probe exhibited a decrease in fluorescence intensity, or a "turn off" response, observed at an emission wavelength of 583 nm.

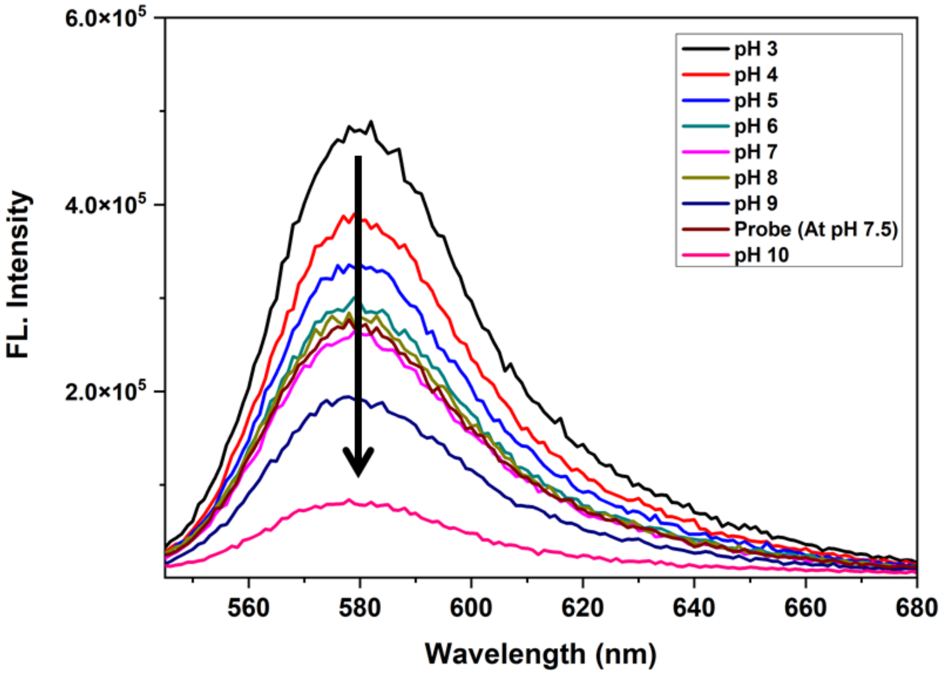

Fig. 15: Fluorescence response of Probe P2 (1 µM) with increasing pH, slit width: excitation/emission = 1/1 nm, HEPES buffer (20 mM, 7.5 pH), Ex: 525 nm.

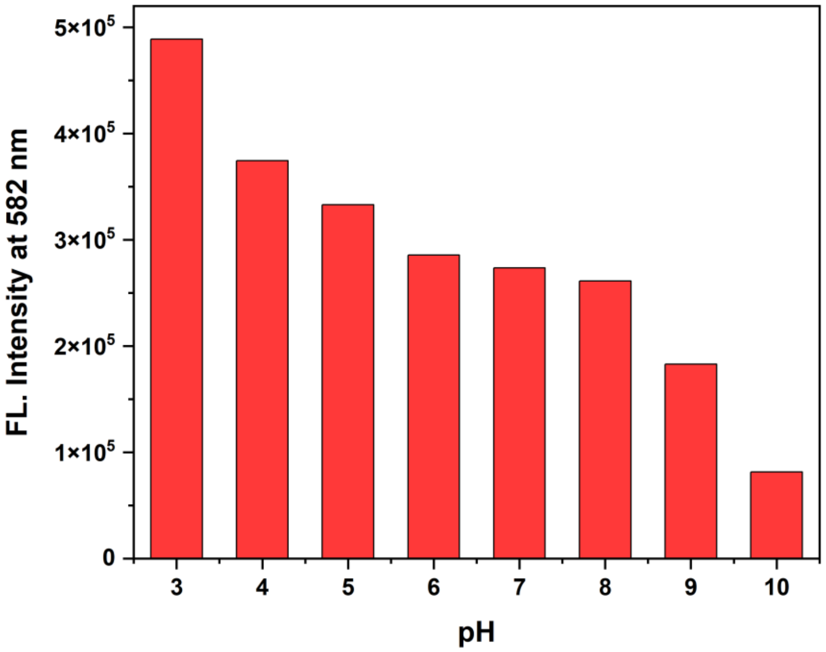

Fig. 16: Bar Plot of Emission Intensity at 582 nm with Increasing Buffer pH

- **Ratiometric response of the Napthalimide based Probe in presence of H_2O_2**

The experiments were conducted using the borylated napthalimide small molecular probe (P2) in 100% DMSO at room temperature. The probe, at a concentration of 10 µM and a volume of 200 µL, was excited at 355 nm. After exposure to 20 µM of H2O2 for 10 minutes, a ratiometric response was detected. This response was characterized by a decrease in emission intensity at 390 nm and a simultaneous increase in intensity at 551 nm.

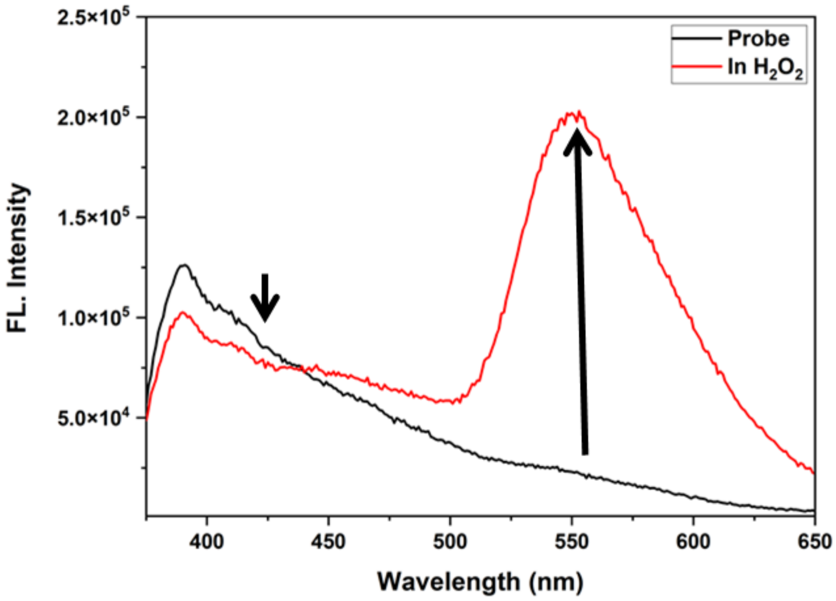

Fig. 17: Ratiometric response of the Napthalimide based Probe in presence of H_2O_2, slit width: excitation/emission = 5/5 nm, 100% DMSO, Ex: 355 nm.

- **LC-MS of the Probe P1**

To track the reaction progress, we conducted liquid chromatography (LC) on the crude reaction mixture using a solvent system and gradient akin to Probe P2. The LC traces exhibited comparable PDA absorbance profiles, with the only distinction being a 10 nm difference in the absorbance wavelength of the band corresponding to the Napthalimide. The yield of the reaction was on the lower side.

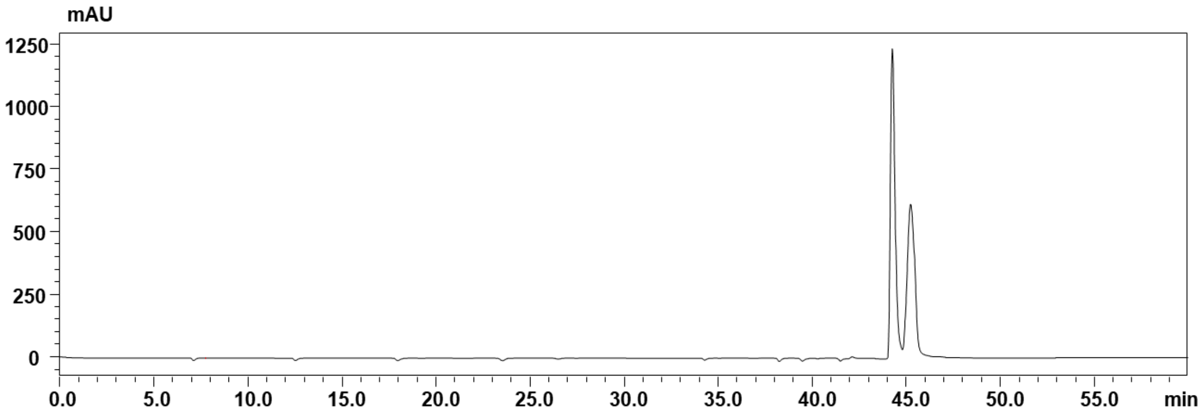

- **Photodiode Array Detector (PDA) Absorbance Profile of the Crude Probe P1 after LC**

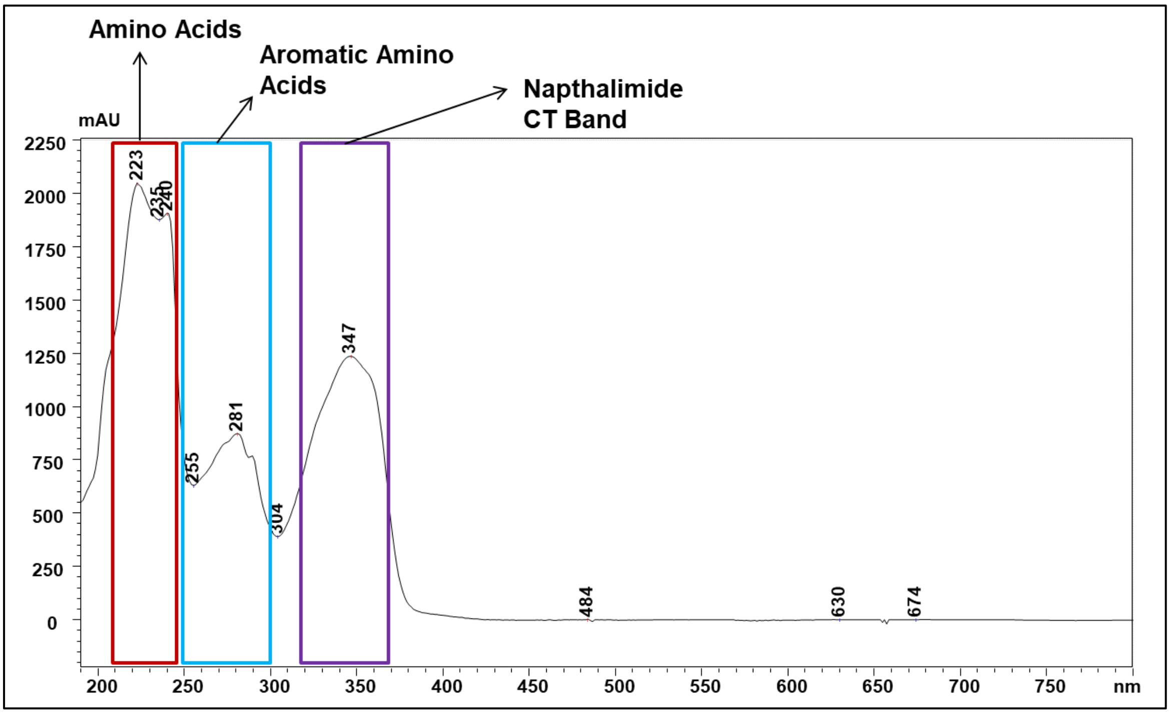

Further optimization of the reaction is required, despite observing interesting results in the LC trace. The PDA absorbance plot indicates the attachment of the Napthalimide moiety to the peptide, although no ESI-MS mass fragments could be obtained. Although in the HRMS data, two mass fragments could be observed. Attached below are several images depicting the visual detection of H_2O_2 by the water soluble probe. Additionally, there is an image showing the bead cleaved Probe P1, exhibiting cyan fluorescence under long-range UV light (365 nm).

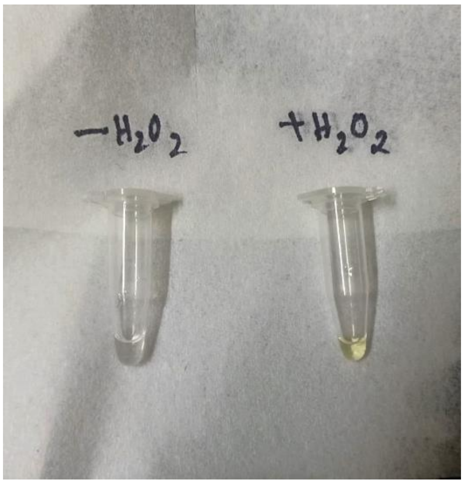

2.5 Conclusion and Future Directions

In this chapter, an attempt was made to synthesize two probes to live track the proton and H_2O_2 concentration of the autophagic vesicles. The probe containing Rhodamine was successfully synthesized and characterized. Further optimization is required for attaching the Napthalimide-containing dye to the autophagy-targeted peptide. A proton concentration-dependent fluorescent titration of the probe (P2) was conducted. Furthermore, fluorescence experiments were conducted to visualize the ratiometric shift of the small molecular probe in presence of H_2O_2. Additionally, a cell penetrability experiment involving the Rhodamine-containing probe can be performed. As a future direction for this project, an orthogonal dual dye-labeled probe could be designed to more effectively track the correlated dynamics of both analytes. Autophagosome formation could also be investigated utilizing microtubule-associated protein light chain 3 (LC3) as a marker in imaging experiments.

References

1. Kim, H., & Seong, J. (2021). Fluorescent Protein-Based Autophagy biosensors. Materials, 14(11), 3019. https://doi.org/10.3390/ma14113019
2. Das, S., Kapadia, A., Pal, S., & Datta, A. (2021). Spatio-Temporal Autophagy Tracking with a Cell-Permeable, Water-Soluble, Peptide-Based, Autophagic Vesicle-Targeted Sensor. ACS Sensors, 6(6), 2252–2260. https://doi.org/10.1021/acssensors.1c00191
3. Lippert, A. R., Van De Bittner, G. C., & Chang, C. J. (2011). Boronate oxidation as a bioorthogonal reaction approach for studying the chemistry of hydrogen peroxide in living systems. Accounts of Chemical Research, 44(9), 793–804. https://doi.org/10.1021/ar200126t
4. Miller, E. W., Dickinson, B. C., & Chang, C. J. (2010). Aquaporin-3 mediates hydrogen peroxide uptake to regulate downstream intracellular signaling. Proceedings of the National Academy of Sciences of the United States of America, 107(36), 15681–15686. https://doi.org/10.1073/pnas.1005776107
5. Van De Bittner, G. C., Dubikovskaya, E. A., Bertozzi, C. R., & Chang, C. J. (2010). In vivo imaging of hydrogen peroxide production in a murine tumor model with a chemoselective bioluminescent reporter. Proceedings of the

National Academy of Sciences of the United States of America, 107(50), 21316–21321. https://doi.org/10.1073/pnas.1012864107

6. Xu, J., Li, Q., Yue, Y., Guo, Y., & Shao, S. (2014). A water-soluble BODIPY derivative as a highly selective “Turn-On” fluorescent sensor for H2O2 sensing in vivo. Biosensors and Bioelectronics, 56, 58–63. https://doi.org/10.1016/j.bios.2013.12.065
7. Karton-Lifshin, N., Segal, E., Omer, L. M. O., Portnoy, M., Satchi-Fainaro, R., & Shabat, D. (2011). A unique paradigm for a Turn-ON Near-Infrared Cyanine-Based probe: noninvasive intravital optical imaging of hydrogen peroxide. Journal of the American Chemical Society, 133(28), 10960–10965. https://doi.org/10.1021/ja203145v
8. Abo, M., Urano, Y., Hanaoka, K., Terai, T., Komatsu, T., & Nagano, T. (2011). Development of a highly sensitive fluorescence probe for hydrogen peroxide. Journal of the American Chemical Society, 133(27), 10629–10637. https://doi.org/10.1021/ja203521e
9. Winterbourn, C. C. (2014). The challenges of using fluorescent probes to detect and quantify specific reactive oxygen species in living cells. Biochimica Et Biophysica Acta (BBA) - General Subjects, 1840(2), 730–738. https://doi.org/10.1016/j.bbagen.2013.05.004
10. Wen, Y., Liu, K., Yang, H., Li, Y., Lan, H., Liu, Y., Zhang, X., & Yi, T. (2014b). A highly sensitive ratiometric fluorescent probe for the detection of cytoplasmic and nuclear hydrogen peroxide. Analytical Chemistry, 86(19), 9970–9976. https://doi.org/10.1021/ac502909c
11. Levine, B., Mizushima, N., & Virgin, H. W. (2011). Autophagy in immunity and inflammation. Nature, 469(7330), 323–335. https://doi.org/10.1038/nature09782
12. Noda, N. N., Ohsumi, Y., & Inagaki, F. (2010). Atg8-family interacting motif crucial for selective autophagy. FEBS Letters, 584(7), 1379–1385. https://doi.org/10.1016/j.febslet.2010.01.018
13. Reggiori, F., Komatsu, M., Finley, K. D., & Simonsen, A. (2012). Autophagy: more than a nonselective pathway. International Journal of Cell Biology, 2012, 1–18. https://doi.org/10.1155/2012/219625
14. Allolio, C., Magarkar, A., Jurkiewicz, R., Ziegler, C., Schröfel, A., & Jungwirth, P. (2018). Arginine-rich cell-penetrating peptides induce membrane

multilamellarity and subsequently enter via formation of a fusion pore. Proceedings of the National Academy of Sciences of the United States of America, 115(47), 11923–11928. https://doi.org/10.1073/pnas.1811520115

15. Wen, Y., Liu, K., Yang, H., Li, Y., Lan, H., Liu, Y., Zhang, X., & Yi, T. (2014). A highly sensitive ratiometric fluorescent probe for the detection of cytoplasmic and nuclear hydrogen peroxide. Analytical Chemistry, 86(19), 9970–9976. https://doi.org/10.1021/ac502909c
16. Shang, L., Xu, X., Qiao, D., Yin, Z., & Shang, L. (2017). Dual mechanism of an intramolecular charge transfer (ICT)–FRET-Based fluorescent probe for the selective detection of hydrogen peroxide. Chemistry-An Asian Journal, 12(24), 3187–3194. https://doi.org/10.1002/asia.201701382
17. Srikun, D., Miller, E. W., Domaille, D. W., & Chang, C. J. (2008). An ICT-Based approach to ratiometric fluorescence imaging of hydrogen peroxide produced in living cells. Journal of the American Chemical Society, 130(14), 4596–4597. https://doi.org/10.1021/ja711480f
18. Li, Z., Niu, C., Liu, Y., Gao, P., Huang, G., & Mao, Y. (2006). A novel fluorescence ratiometric pH sensor based on covalently immobilized piperazinyl-1,8-napthalimide and benzothioxanthene. Sensors and Actuators B: Chemical, 114(1), 308–315. https://doi.org/10.1016/j.snb.2005.05.018
19. Pfeffer, F. M., Seter, M., Lewcenko, N. A., & Barnett, N. W. (2006). Fluorescent anion sensors based on 4-amino-1,8-naphthalimide that employ the 4-amino N–H. Tetrahedron Letters, 47(30), 5241–5245. https://doi.org/10.1016/j.tetlet.2006.05.161
20. Liu, B., & Tian, H. (2005). A selective fluorescent ratiometric chemodosimeter for mercury ion. Chemical Communications, 25, 3156. https://doi.org/10.1039/b501913c
21. Bakthavatsalam, S., Sarkar, A., Rakshit, A., Jain, S., Kumar, A., & Datta, A. (2015). Tuning macrocycles to design 'turn-on' fluorescence probes for manganese(II) sensing in live cells. Chemical Communications, 51(13), 2605–2608. https://doi.org/10.1039/C4CC09542A
22. Parkesh, R., Lee, T. C., & Gunnlaugsson, T. (2007). Highly selective 4-amino-1,8-naphthalimide based fluorescent photoinduced electron transfer (PET) chemosensors for Zn(ii) under physiological pH conditions. Organic and Biomolecular Chemistry, 5(2), 310–317. https://doi.org/10.1039/b614529a

23. Wang, J., Jin, S., Akay, S., & Wang, B. (2007). Design and Synthesis of Long-Wavelength Fluorescent Boronic Acid Reporter Compounds. European Journal of Organic Chemistry, 2007(13), 2091–2099. https://doi.org/10.1002/ejoc.200700008
24. Simon, M. D., Heider, P. L., Adamo, A., Vinogradov, A. A., Mong, S. K., Li, X., Berger, T., Policarpo, R. L., Zhang, C., Zou, Y., Liao, X., Spokoyny, A. M., Jensen, K. F., & Pentelute, B. L. (2014). Rapid Flow-Based peptide synthesis. ChemBioChem, 15(5), 713–720. https://doi.org/10.1002/cbic.201300796
25. Dèng, F., Sun, D., Yang, S., Huang, W., Huang, C., Xu, Z., & Liu, L. (2022). Comparison of rhodamine 6G, rhodamine B and rhodamine 101 spirolactam based fluorescent probes: A case of pH detection. Spectrochimica Acta Part A: Molecular and Biomolecular Spectroscopy, 268, 120662. https://doi.org/10.1016/j.saa.2021.120662
26. Shen, S., Zhang, X., Ge, Y., Zhu, Y., Lang, X., & Cao, X. (2018). A near-infrared lysosomal pH probe based on rhodamine derivative. Sensors and Actuators B: Chemical, 256, 261–267. https://doi.org/10.1016/j.snb.2017.10.103

Chapter 3: Computational Calculations on the Naphthalimide ROS Probe

3.1 Introduction

Our technique for ratiometric fluorescence detection of cellular hydrogen peroxide (H_2O_2) entails controlling intramolecular charge transfer (ICT) within a dye platform to induce a shift in emission wavelength upon interaction with H_2O_2. We finely tune the electron-donating hydroxyl group positioned at the 4-position of a 1,8-naphthalimide, which impacts both intramolecular charge transfer (ICT) and the emitted wavelength. Blue shifts in emission observed with more electron-deficient substituents at the above-mentioned position. Replacing the 4-hydroxyl donor with a more substantial electron-withdrawing boronic ester group, which H_2O_2 can precisely remove back to the hydroxyl, would allow for ratiometric detection of H_2O_2. This ratiometric technique resembles the indicators for non-genetically encoded analytes such as pH, anions, metal ions, and sugars [2-7].

ICT probes use a single fluorophore, resulting in a smaller, less stiff probe. When the boronic ester is absent, the naphthalimide probe has both an electron-donating and an electron-withdrawing group, increasing stability and lowering the energy of the internal charge transfer excited state. However, when the hydroxyl group is replaced with a boronic ester molecule, the ICT state's push-pull mechanism is broken, resulting in a blue-shifted fluorescence emission from the more stable excited state [7].

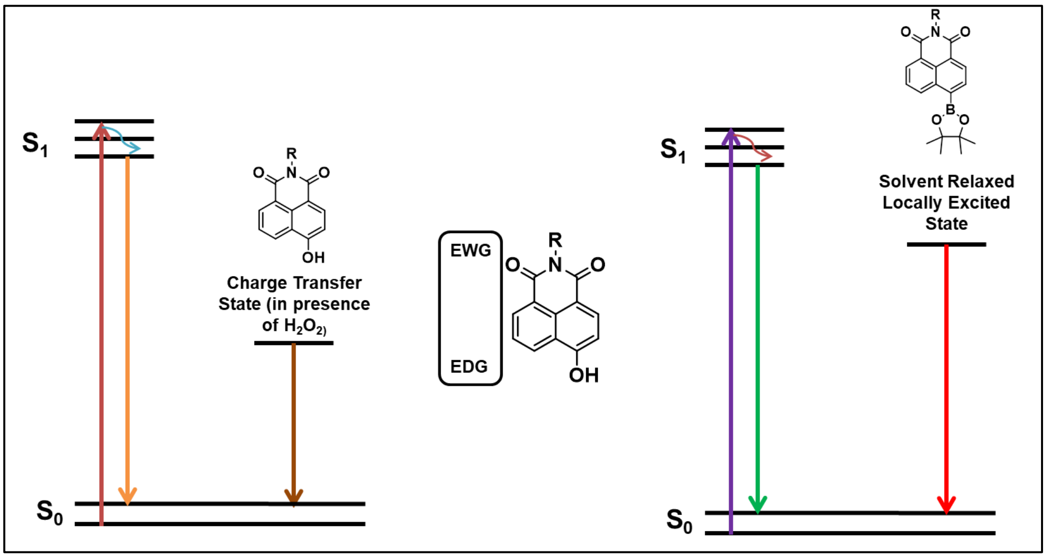

Fig. 18: ICT Mechanism Utilizing the Jablonski Diagram

This chapter of the thesis will encompass the utilization of DFT and TD-DFT computations [8]. The goal is to examine and get a deeper understanding of the feasibility of Intramolecular Charge Transfer (ICT) within our Napthalimide-based probe, as described in the previous chapter. The theoretical predictions' outcomes will be a major focus of this chapter's discussion.

3.2 Materials and Methods

The geometry optimization process commenced with a planar structure of the sensor generated through GaussView 6.0.18 software. Ground state geometries of the molecules underwent vacuum DFT geometry optimizations, employing the B3LYP exchange-correlational functional and the 6-311++G(d,p) basis set in Gaussian 16 software [8]. Subsequently, Frontier Molecular Orbitals (MOs) were obtained for the DFT optimized ground state geometries. TD-DFT calculations were conducted on these optimized geometries to ascertain details regarding the initial and final electronic states of the most likely transitions, focusing on their MO composition. Each case considered a total of 50 states. The transitions with the highest oscillation strength and transition probability were regarded as the most probable transitions. Both DFT and TD-DFT calculations employed the B3LYP exchange-correlational functional and the 6-311++G(d,p) basis set within Gaussian 16 software. Solvent effects, simulated through a polarizable continuum model (PCM), were taken into account [8].

3.3 Results and Discussions

First, DFT calculations (using B3LYP with the 6-311++G(d,p) basis set) were performed on both the borylated and phenolic-OH forms of the dye in a water environment. Electron density maps were then constructed for each molecule using the DFT calculation results (optimized geometries). The Avogadro software was used to visualise these electron density maps. A subset of obtained states from HOMO - 3 to LUMO + 3 are reported below, in two distinct diagrams for visualization purposes.

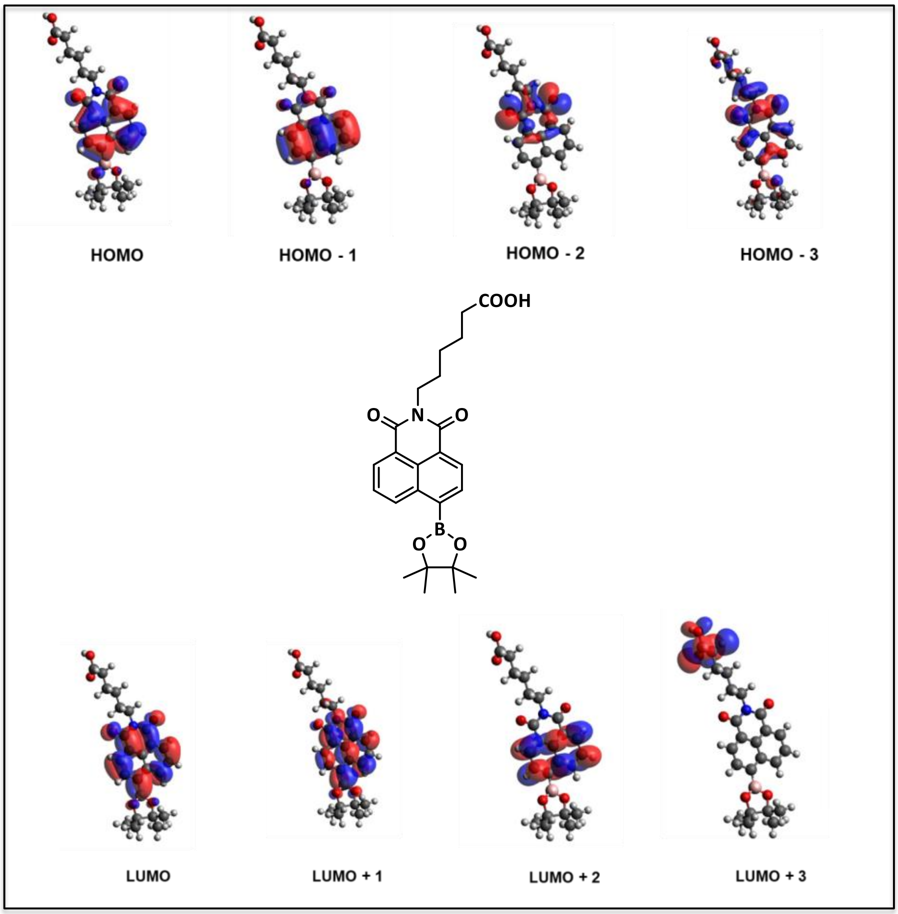

Fig. 19: Electron Density Maps of Borylated Molecule

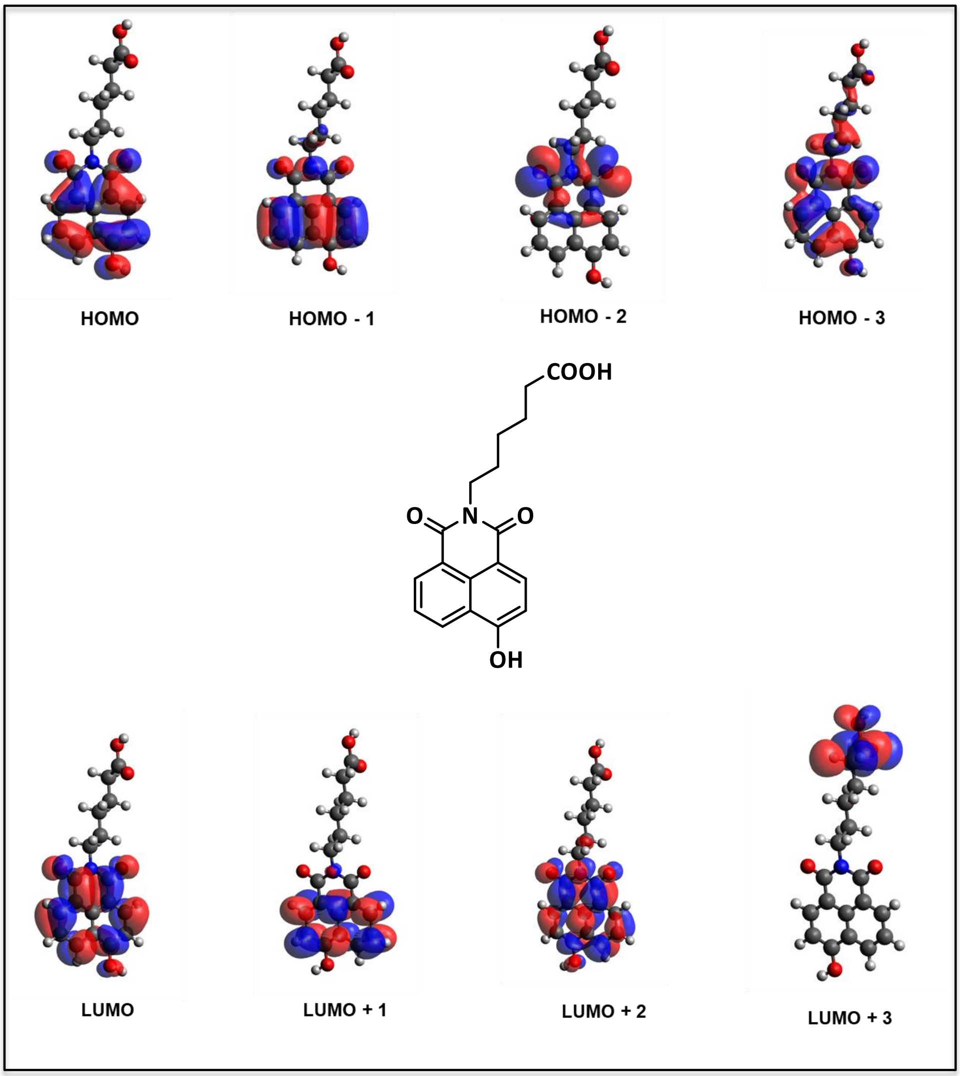

Fig. 20: Electron Density Maps of Hydroxyl Donor Molecule

Secondly, TD-DFT calculations were conducted using the DFT optimized geometries of both molecules to identify the most likely transition states. In the borylated molecule, the primary transition state occurs from the HOMO at -6.74 eV to the LUMO +2 at -1.02 eV. In case of the hydroxyl donor molecule, the most probable transition state is from HOMO (-6.45 V) to LUMO (-2.71 eV). Although electron density maps show no apparent Intramolecular Charge Transfer (ICT) due to absence of charge separation, an intriguing observation emerges from the TD-DFT results. Specifically, a decrease in the energy gap during the most likely transition state implies a red-shifted absorption in the hydroxyl donor molecule. These findings, as summarised in the accompanying figure, suggest a promising avenue for future research into charge transfer processes.

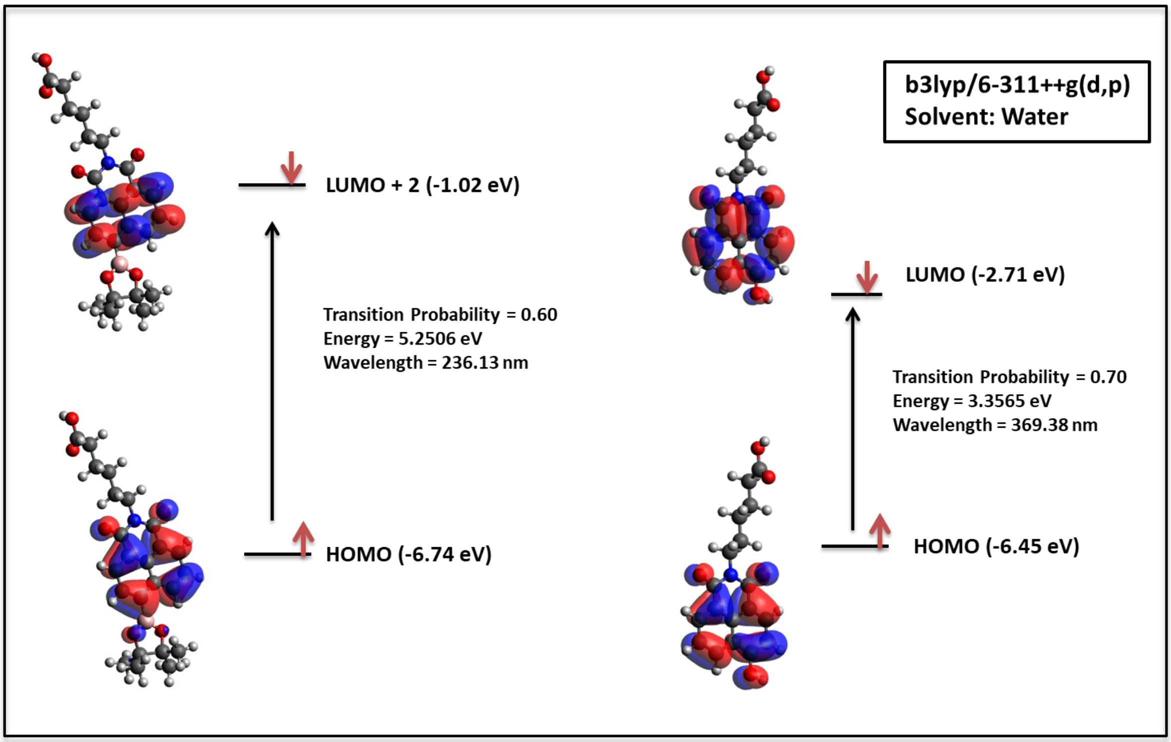

Fig. 21: Summarizing the TD-DFT Calculations

3.4 Conclusion and Future Directions

This chapter presents the first time utilization of DFT and TD-DFT calculations on a synthesized small molecular probe. While DFT electron density maps did not reveal significant charge separation attributable to Intramolecular Charge Transfer (ICT), TD-DFT analysis indicated a reduction in the energy gap during the most probable transition of the hydroxyl donor molecule. Looking ahead, future research endeavors could validate this hypothesis through re-calculating computations in different solvents with varying dielectric constants, particularly at higher transition states.

3.5 References

1. Srikun, D., Miller, E. W., Domaille, D. W., & Chang, C. J. (2008). An ICT-Based approach to ratiometric fluorescence imaging of hydrogen peroxide produced in living cells. Journal of the American Chemical Society, 130(14), 4596–4597. https://doi.org/10.1021/ja711480f
2. Li, Z., Niu, C., Liu, Y., Gao, P., Huang, G., & Mao, Y. (2006). A novel fluorescence ratiometric pH sensor based on covalently immobilized

piperazinyl-1,8-napthalimide and benzothioxanthene. Sensors and Actuators B: Chemical, 114(1), 308–315. https://doi.org/10.1016/j.snb.2005.05.018

3. Pfeffer, F. M., Seter, M., Lewcenko, N. A., & Barnett, N. W. (2006). Fluorescent anion sensors based on 4-amino-1,8-naphthalimide that employ the 4-amino N–H. Tetrahedron Letters, 47(30), 5241–5245. https://doi.org/10.1016/j.tetlet.2006.05.161
4. Liu, B., & Tian, H. (2005). A selective fluorescent ratiometric chemodosimeter for mercury ion. Chemical Communications, 25, 3156. https://doi.org/10.1039/b501913c
5. Bakthavatsalam, S., Sarkar, A., Rakshit, A., Jain, S., Kumar, A., & Datta, A. (2015). Tuning macrocycles to design ‘turn-on’ fluorescence probes for manganese(II) sensing in live cells. Chemical Communications, 51(13), 2605–2608. https://doi.org/10.1039/C4CC09542A
6. Parkesh, R., Lee, T. C., & Gunnlaugsson, T. (2007). Highly selective 4-amino-1,8-naphthalimide based fluorescent photoinduced electron transfer (PET) chemosensors for Zn(ii) under physiological pH conditions. Organic and Biomolecular Chemistry, 5(2), 310–317. https://doi.org/10.1039/b614529a
7. Wang, J., Jin, S., Akay, S., & Wang, B. (2007). Design and Synthesis of Long-Wavelength Fluorescent Boronic Acid Reporter Compounds. European Journal of Organic Chemistry, 2007(13), 2091–2099. https://doi.org/10.1002/ejoc.200700008
8. Kahali, S. 2021, Chapter-2 (Predicting the Possibility of PET in a Series of Novel Apo-Sensors). Evaluating Design Criteria for Photo-induced Electron Transfer (PET) based “Turn-on” Reversible Fluorescent Mn2+ Sensors.

Chapter 4: Toward Mitochondrial-Targeted Sensors for ROS and pH Detection

4.1 Introduction

In this chapter, an attempt has been made to develop peptide based sensors designed to detect ROS and pH levels within mitochondria. Using the methods described in Chapter 2, a small molecule probe for ROS detection was synthesized. Additionally, Rhodamine was used as the pH-sensitive dye for precise pH sensing. The aim was to add both the sensors simultaneously in living cells for co-localized imaging studies to live track both the analytes in the mitochondria. The detailed design is elaborated in the results section

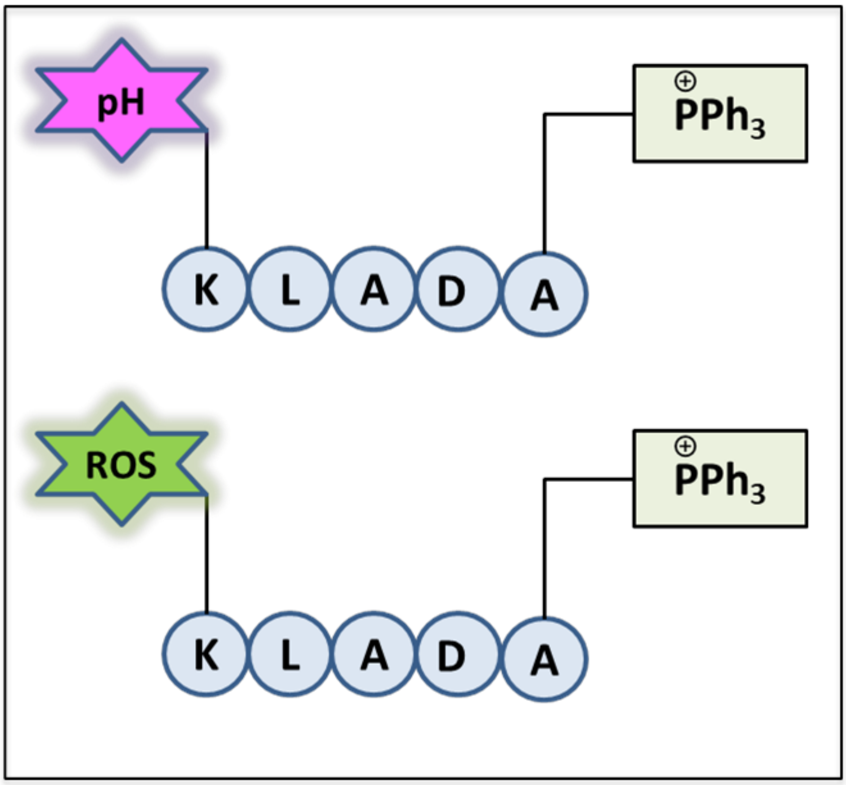

Fig. 22: The Mitochondrial-Targeted pH and ROS Sensor Designs

4.2 Materials

Similar materials were utilized in this chapter as in the previous one.

4.3 Methods

Overall Scheme

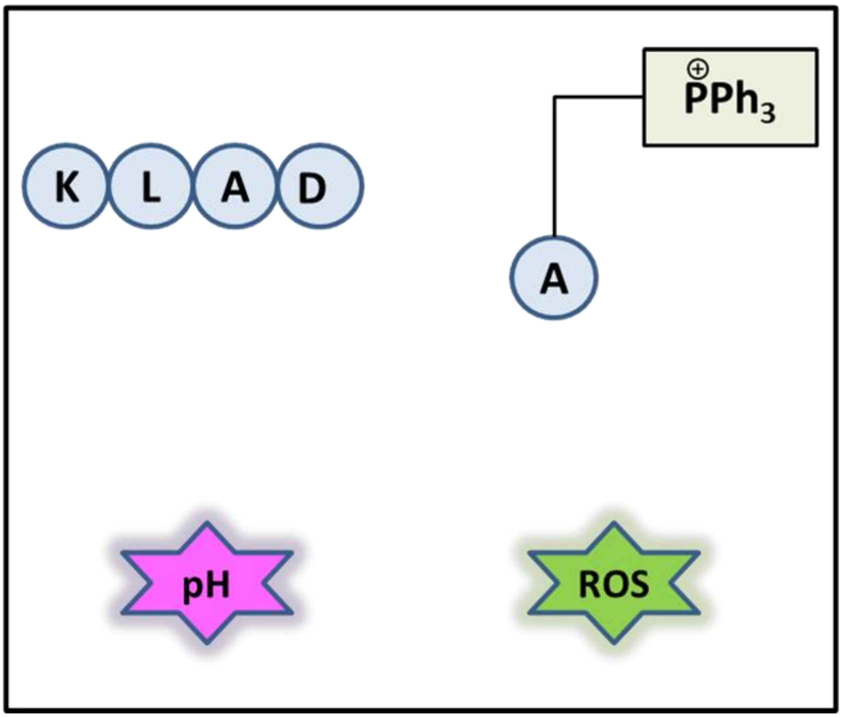

- **Synthesis of KLAD**

Procedure: As Reported Earlier Chapter 2.

LRMS: m/z Calculated (M)= 706, Observed ($[M+H]^+$, $[M+Na^+]$) = 707, 729

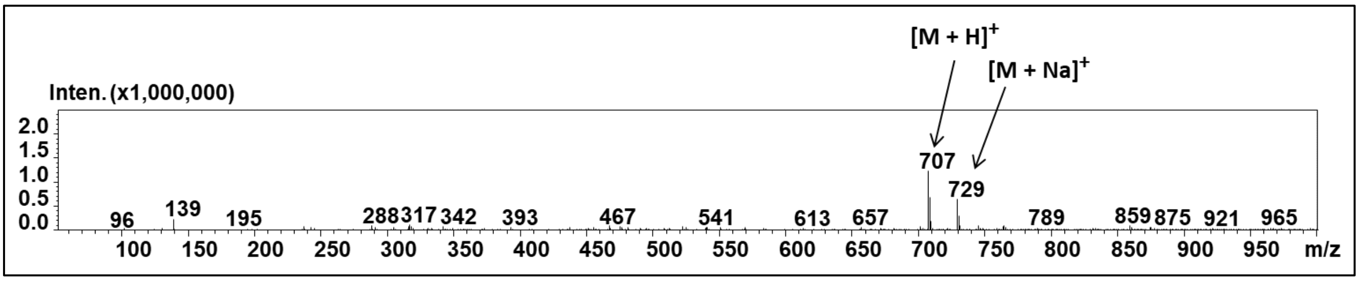

- **Allyl Group Deprotection of KLAD**

Procedure:

Peptide(KLAD) synthesized on-bead (14 mg, 0.021 mmol) was washed with dichloromethane (DCM) for 15 minutes. A solution of dimethylphenylsilane (96 μL, 0.63 mmol) in 150 μL DCM was added to the beads and stirred in a rotor 15 minutes. Subsequently, a solution of palladium(0) triphenylphosphine ($Pd(PPh_3)_4$) (7 mg, 0.0063 mmol) in 600 μL DCM was added to the beads under Argon and the reaction mixture was stirred in the rotor for 45 minutes. After 45 minutes, the beads were quickly washed multiple times with DCM and Methanol and dried to give the molecule on bead. The allyl deprotected peptide was cleaved from the bead to confirm the successful deprotection.

LRMS: m/z Calculated (M)= 667, Observed (M^+) = 667

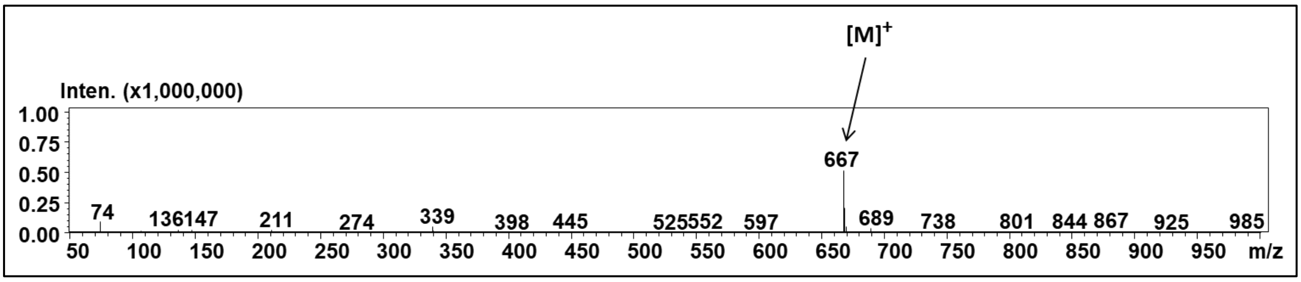

- **Synthesis of the Clickable Precursor**

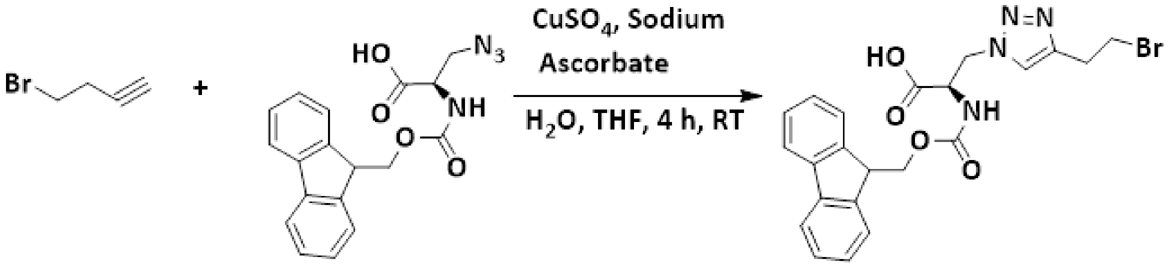

Procedure: Copper(II) sulphate pentahydrate (5 mg, 0.042 mmol) and Sodium L-ascorbate (7.39 mg, 0.019 mmol) was dissolved in degassed water (2 mL each) separately. Then both solutions were taken in a three neck round bottomed flask under Argon. The solution changes colour from deep brown to light orange. The alkyne (5 mg, 0.038 mmol) and azide (33 mg, 0.093 mmol) compound were dissolved in degassed Tetrahydrofuran (10 mL) and was added to the reaction mixture consisting of the active catalyst. The reaction was kept at room temperature for 4 hours. The solvent was dried under vacuum followed by filtration in sodium sulphate.

LRMS: m/z Calculated (M) = 484, Observed ($[M+H]^+$) = 485

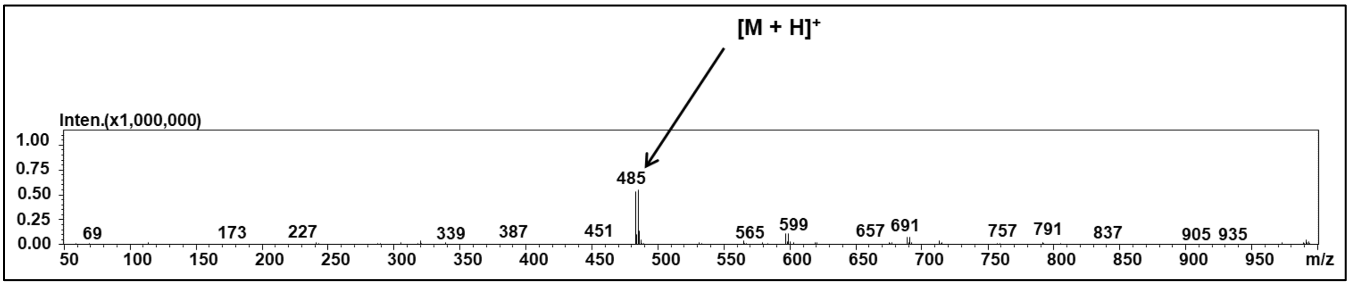

- **Synthesis of Mitochondrial Targetting Moiety**

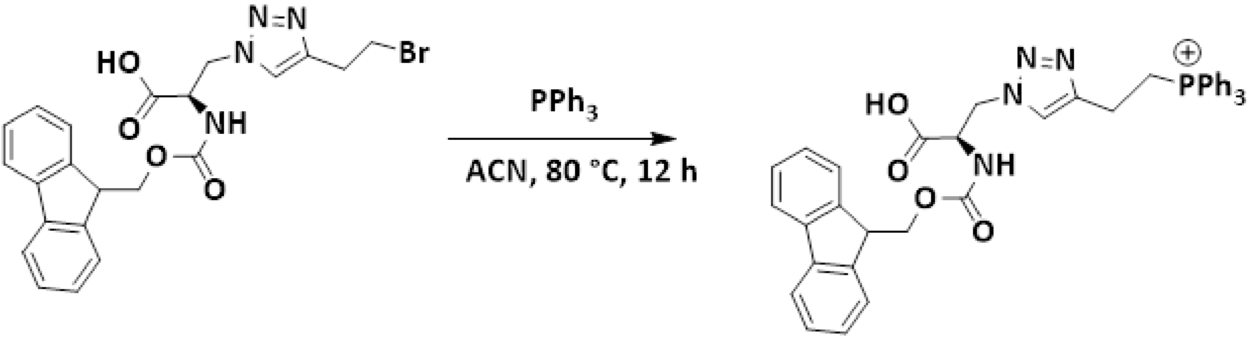

Procedure: The starting material (20 mg, 0.04 mmole) was dissolved in Acetonitrile (30 mL) and followed by addition of Triphenylphosphine (33 mg, 0.12 mmole) in a dropwise manner. The reaction mixture was refluxed overnight at 80°C. After cooling to room temperature, solvent removal was achieved using a rotary evaporator.

LRMS: m/z Calculated = 667 (M^+), Observed (M^+) = 667

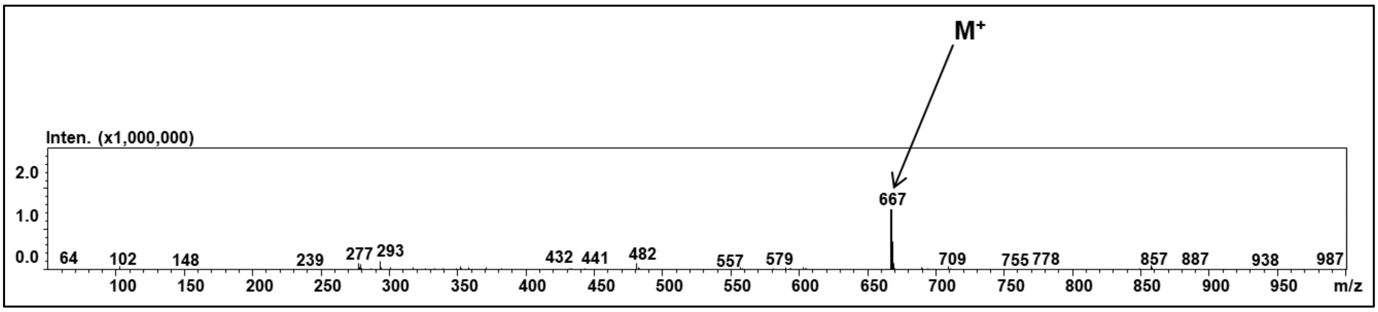

- **Attachment of pH Sensitive Dye to the KLAD Peptide**

Procedure: As Reported Earlier Chapter 2.

LRMS: m/z Calculated (M)= 896, Observed ($[M+K]^+$) = 935

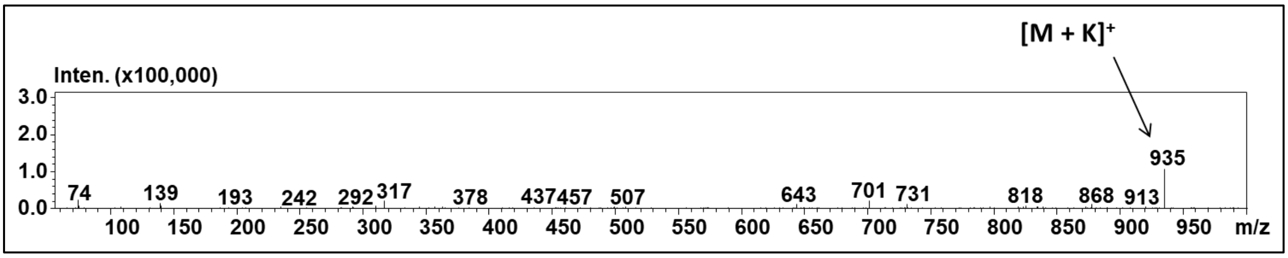

4.4 Results and Discussion

In this chapter, a shorter peptide was selected that includes Lysine (K), Leucine (L), and Alanine (A) to improve cell permeability. Aspartic acid (D) was positioned at the C-terminus of the peptide for linking to the bead via its side chain, while the main terminus was protected by an allyl protecting group. This design was chosen to facilitate the attachment of a mitochondrial targeting group, specifically triphenyl phosphine-modified Alanine (A). The positive charge of the triphenyl phosphine also aids in cellular uptake and water solubility enhancement. The rhodamine dye and hydrogen peroxide probe would be connected to the primary chain of Lysine at the N-terminus after removal of the Fmoc protecting group. All these coupling reactions were conducted on the bead as part of a solid-phase synthetic approach to ensure better yields.

4.5 Conclusion and Future Directions

The earlier discussed component units, synthesized individually, can be combined to form the final sensor, which is then ready to detect analytes. The probe can be used for in-vitro titration experiments and finally for live cell imaging.

Chapter 5: Overall Summary and Future Perspectives

In Chapter 2, a ratiometric sensor has been synthesized to detect endogenous hydrogen peroxide levels in Autophagic Vesicles. Also, to facilitate the co-localization imaging studies a Rhodamine dye attached sensor was synthesized to track the proton concentration levels in Autophagic Vesicles. In the subsequent chapter, computational calculations of the Naphthalimide-based small molecular probe were performed to understand its spectrochemical properties.

In Chapter 4, an attempt has been made to develop sensors for detecting pH and ROS in Mitochondria. However, a future perspective of this project could involve the development of a single sensor capable of detecting both analytes. This could be achieved by employing various peptide ligation methods, thereby enhancing the versatility and efficiency of the sensor.

Finally, the live cell imaging studies using both the mitochondrial and autophagosome targeted sensors will be performed to better understand the correlated dynamics of non-genetically encoded analytes.

APPENDIX

- **Precursor of the ROS Probe ^{1}H NMR**

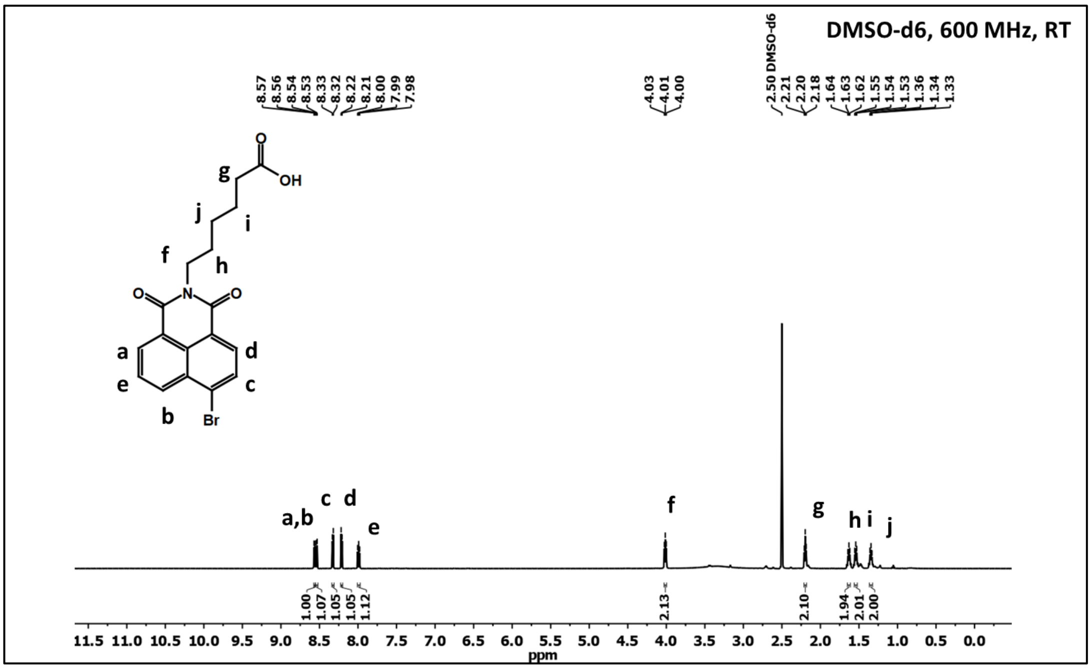

- **ROS Probe ^{1}H NMR**

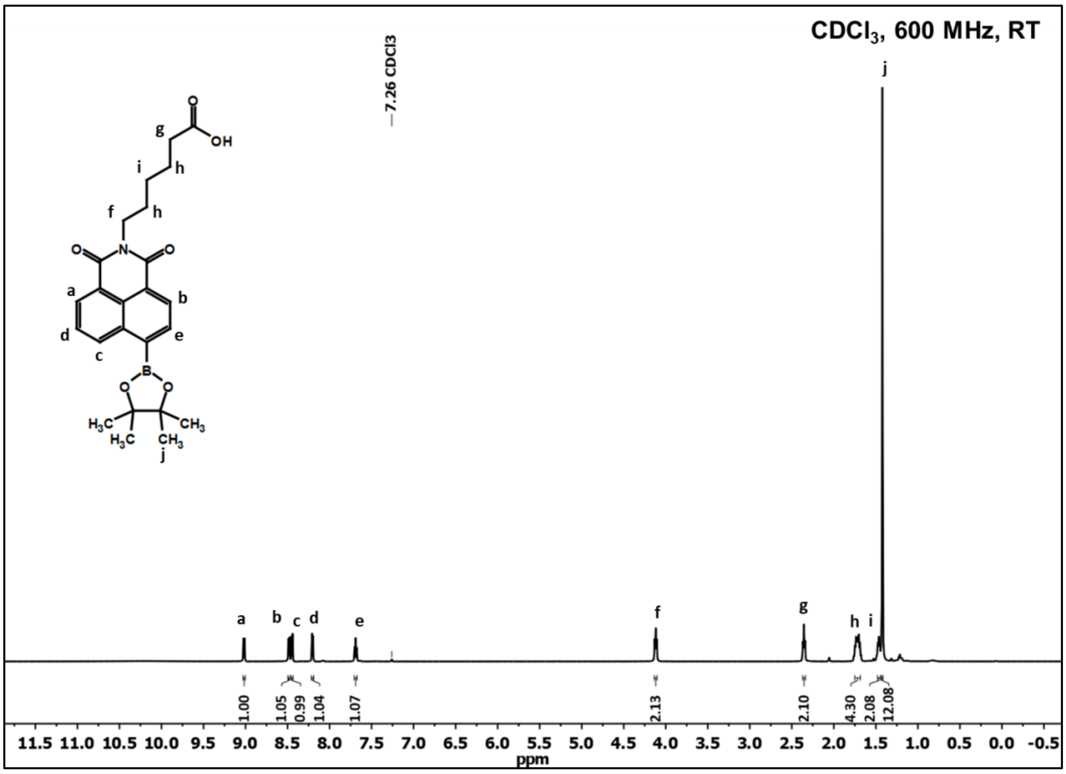

- **ROS Probe ^{13}C NMR**

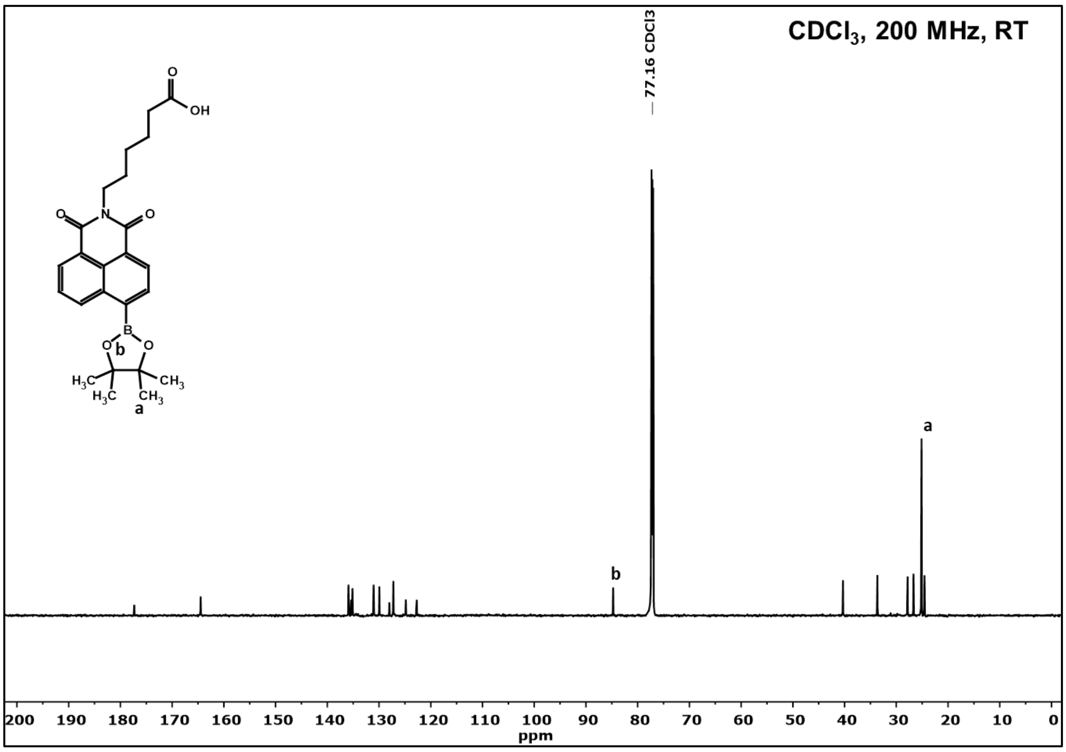

- **MALDI MS of the Autophagy Peptide**

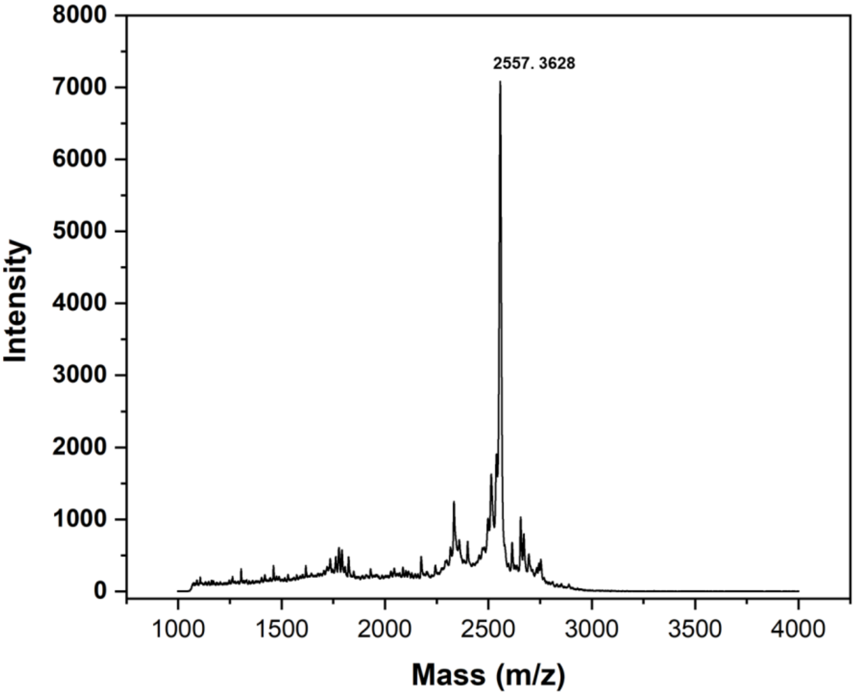

- **HRMS of Probe (P1)**

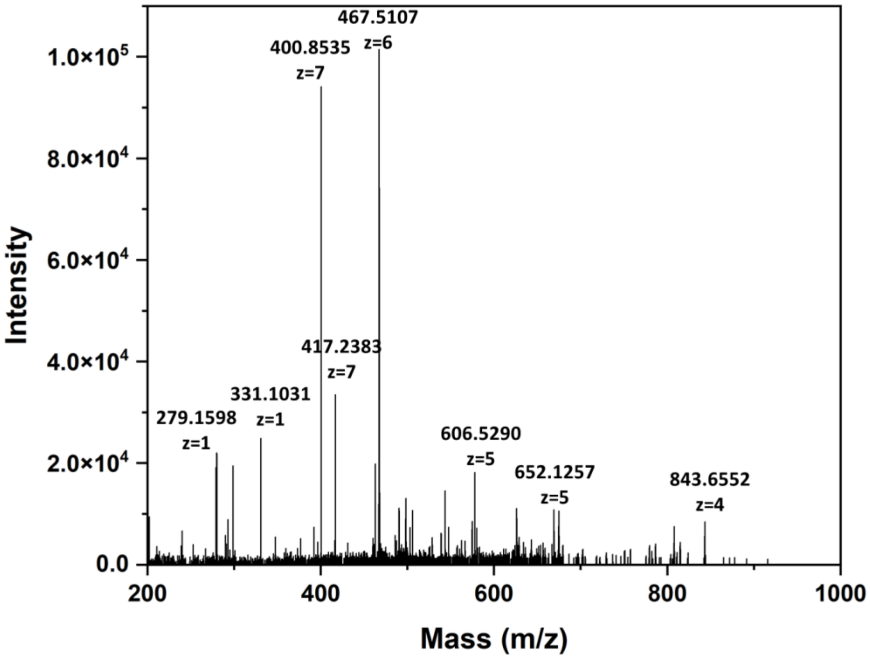

---------xx----------